Author Manuscript

Author Manuscript

Author Manuscript

Author Manuscript

HHS Public Access

Author manuscript

Cell. Author manuscript; available in PMC 2019 June 28.

Published in final edited form as:

Cell. 2018 June 28; 174(1): 102–116.e14. doi:10.1016/j.cell.2018.04.035.

CTCF-Binding Elements Mediate Accessibility of RAG Substrates During Chromatin Scanning

Suvi Jain[1,2,3], **Zhaoqing Ba**[1,2,3], **Yu Zhang**[1,2], **Hai-Qiang Dai**[1,2], and **Frederick W. Alt**[1,2,4,*]

[1]Howard Hughes Medical Institute

[2]Program in Cellular and Molecular Medicine, Boston Children's Hospital, and Department of Genetics, Harvard Medical School, Boston, MA 02115, USA

SUMMARY

RAG endonuclease initiates antibody heavy chain variable region exon assembly from V, D, and J segments within a chromosomal V(D)J recombination center (RC) by cleaving between paired gene segments and flanking recombination signal sequences (RSSs). The IGCR1 control region promotes DJ_H intermediate formation by isolating Ds, J_Hs, and RCs from upstream V_Hs in a chromatin loop anchored by CTCF-binding elements (CBEs). How V_Hs access the DJ_HRC for V_H to DJ_H rearrangement was unknown. We report that CBEs immediately downstream of frequently rearranged V_H-RSSs increase recombination potential of their associated V_H far beyond that provided by RSSs alone. This CBE activity becomes particularly striking upon IGCR1 inactivation, which allows RAG, likely via loop extrusion, to linearly scan chromatin far upstream. V_H-associated CBEs stabilize interactions of D-proximal V_Hs first encountered by the DJ_HRC during linear RAG scanning and thereby promote dominant rearrangement of these V_Hs by an unanticipated chromatin accessibility-enhancing CBE function.

Graphical abstract

In Brief: RAG endonuclease associated with a DJ_H recombination center is presented with upstream chromosomal V_Hs by a linear chromatin scanning process involving loop extrusion. During this process, V_H-proximal CTCF looping factor binding elements mediate greatly increased interactions of their associated V_Hs with the DJ_H recombination center and, thereby, increase their accessibility for RAG cleavage and subsequent V(D)J recombination.

*Correspondence: alt@enders.tch.harvard.edu.

[3]These authors contributed equally

[4]Lead Contact

SUPPLEMENTAL INFORMATION

Supplemental Information includes seven figures and five tables and can be found with this article online at https://doi.org/10.1016/j.cell.2018.04.035.

AUTHOR CONTRIBUTIONS

S.J., Z.B., and F.W.A. designed the study. S.J. made the various mutant *v-Abl* and mouse lines and did experiments in collaboration with Z.B. who developed 3C-HTGTS. Y.Z. derived the parental $D_HFL16.1J_H4$ *v-Abl* transformed pro-B cell line and its IGCR1 deleted derivative. H.-Q.D. collaborated on V_H to D_H intergenic deletion experiments. S.J., Z.B., and F.W.A. analyzed and interpreted the data, designed figures, and wrote the manuscript.

DECLARATION OF INTERESTS

The authors declare no competing interests.

Author Manuscript Author Manuscript Author Manuscript Author Manuscript

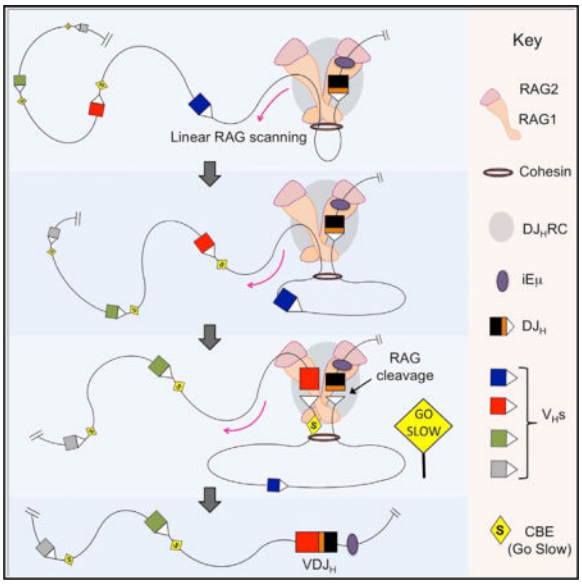

INTRODUCTION

Exons encoding immunoglobulin (Ig) or T cell receptor variable regions are assembled from V, D, and J gene segments during B and T lymphocyte development. V(D)J recombination is initiated by RAG1/RAG2 endonuclease (RAG), which introduces DNA double-stranded breaks (DSBs) between a pair of V, D, and J coding segments and flanking recombination signal sequences (RSSs) (Teng and Schatz, 2015). RSSs consist of a conserved heptamer, closely related to the canonical 5′-CACAGTG-3′ sequence, and a less-conserved nonamer separated by 12 (12RSS) or 23 (23RSS) bp spacers. Physiological RAG cleavage requires RSSs and is restricted to paired coding segments flanked, respectively, by 12RSSs and 23RSSs (Teng and Schatz, 2015). RAG binds paired RSSs as a Y-shaped heterodimer (Kim et al., 2015; Ru et al., 2015), with cleavage occurring adjacent to heptamer CACs. Cleaved coding and RSS ends reside in a RAG post-cleavage synaptic complex prior to fusion of RSS ends and coding ends, respectively, by non-homologous DSB end-joining (Alt et al., 2013).

The mouse Ig heavy chain locus (*Igh*) spans 2.7 Mb, with more than 100 V_Hs flanked by 23RSSs embedded in the 2.4 Mb distal portion; 13 Ds flanked on each side by a 12RSS located in a region starting 100 kb downstream of the D-proximal V_H (V_H5-2; commonly termed "V_H81X"), and 4 J_Hs flanked by 23RSSs lying just downstream of the Ds (Alt et al., 2013) (Figures 1A and S1A). *Igh* V(D)J recombination is ordered, with Ds joining on their downstream side to J_Hs before V_Hs join to the upstream side of the DJ_H intermediate (Alt et al., 2013). D to J_H joining initiates after RAG is recruited to a nascent V(D)J recombination center ("nRC") to form an active V(D)J recombination center (RC) around the *Igh* intronic enhancer (iEm), J_Hs, and proximal D_HQ52 (Teng and Schatz, 2015). Upon formation of DJ_H intermediates, V_Hs must enter a newly established DJ_HRC for joining. In this regard, *Igh* locus contraction brings V_Hs into closer physical proximity to the DJ_HRC, allowing utilization of V_Hs from across the V_H domain (Bossen et al., 2012; Ebert et al., 2015;

Author Manuscript Author Manuscript Author Manuscript Author Manuscript

Proudhon et al., 2015). Following locus contraction, diffusion-related mechanisms contribute to V_H incorporation into the DJ_HRC (Lucas et al., 2014). Yet, diffusion access alone may not explain reproducible variations in relative utilization of individual V_Hs (Lin et al., 2016; Bolland et al., 2016).

V(D)J recombination is regulated to maintain specificity and diversity of antigen receptor repertoires by modulating chromatin accessibility of particular Ig or TCR loci, or regions of these loci, for V(D)J recombination (Yancopoulos et al., 1986; Alt et al., 2013). Accessibility regulation was proposed based on robust transcription of distal V_Hs before rearrangement (Yancopoulos and Alt, 1985) and correlated with various epigenetic modifications (Alt et al., 2013). In this regard, germline transcription and active chromatin modifications in the nRC recruit RAG1 and RAG2 to form the active RC (Teng and Schatz, 2015). Genome organization alterations also positively impact V_H "accessibility" by bringing distal V_Hs into closer physical proximity to the DJ_HRC via *Igh* locus contraction (Bossen et al., 2012). Conversely, the intergenic control region 1 (IGCR1) in the V_H to D interval plays a negative, insulating role with respect to proximal V_H accessibility (Guo et al., 2011). IGCR1 function relies on two CTCF looping factor binding elements ("CBEs") that contribute to sequestering Ds, J_Hs and RC within a chromatin domain that excludes proximal V_Hs; thereby, mediating ordered D to J_H recombination and preventing proximal V_H over-utilization (Guo et al., 2011; Lin et al.; 2015; Hu et al., 2015).

Eukaryotic genomes are organized into Mb or sub-Mb topologically associated domains (TADs) (Dixon et al., 2012; Nora et al., 2012) that often include contact loops anchored by pairs of convergent CBEs bound by CTCF in association with co-hesin (Phillips-Cremins et al., 2013; Rao et al., 2014). In this regard, CTCF binds CBEs in an orientation-dependent fashion. Ability to recognize widely separated convergent CBEs may involve cohesin, or other factors, that progressively extrude a growing chromatin loop that is fixed into a domain upon reaching convergent CTCF-bound loop anchors (Sanborn et al., 2015; Nichols and Corces, 2015; Fudenberg et al., 2016; Dekker and Mirny, 2016). In mammalian cells, CBEs, TADs, and/or loop domains have been implicated in regulation of various physiological processes (Dekker and Mirny, 2016; Merkenschlager and Nora, 2016; Hnisz et al., 2016), with convergent CBE-based loop organization implicated as critical for such regulation in some cases (Sanborn et al., 2015; Guo et al., 2015; de Wit et al., 2015; Ruiz-Velasco et al., 2017).

RAG can explore directionally from an initiating physiological or ectopically introduced RC for Mb distances within convergent CBE-based contact chromatin loop domains genome-wide (Hu et al., 2015). During such exploration, RAG uses RSSs in convergent orientation, including cryptic RSSs as simple as a CAC, for cleavage and joining to a canonical RSS in the RC (Hu et al., 2015; Zhao et al., 2016). This long-range directional RAG activity is impeded upon encounter of cohesin-bound convergent CBE pairs and potentially by other blockages that create chromatin sub-domains within loops (Hu et al., 2015; Zhao et al., 2016). The directionality and linearity of RAG activity across these domains implicated one-dimensional RAG tracking (Hu et al., 2015). Directional RAG tracking also occurs upstream of the DJ_H RC to IGCR1 (Hu et al., 2015). IGCR1 deletion extends this recombination tracking domain directionally upstream of the DJ_H RC to the proximal V_Hs, coupled with

Author Manuscript Author Manuscript Author Manuscript Author Manuscript

dramatically increased proximal V_H to DJ_H joining, most dominantly V_H81X (Hu et al., 2015). However, the nature of the tracked substrate and factors that drive RAG tracking remained speculative.

The mouse *Igh* harbors a high density of CBEs (Degner et al., 2011). Ten clustered CBEs ("3′CBEs") lie at the downstream *Igh* boundary in convergent orientation to more than 100 CBEs embedded across the V_H domain (Proudhon et al., 2015). V_H CBEs are spread throughout the V_H domain and, particularly for more proximal V_Hs, often found immediately downstream of V_H RSSs (Choi et al., 2013; Bolland et al., 2016). Notably, V_H CBEs and 3′CBEs are in convergent orientation with each other and with, respectively, the upstream and downstream IGCR1 CBEs (Guo et al., 2011). The striking number and organization of the CBEs across the V_H portion of *Igh* has led to speculation of potential positive or negative V_H CBE roles in *Igh* V(D)J recom bination (Bossen et al., 2012; Guo et al., 2011; Benner et al., 2015; Degner et al., 2011; Lin et al., 2015). Our current studies reveal the function of proximal V_H CBEs and provide new insights into the RAG tracking mechanism.

RESULTS

The V_H81X-CBE Greatly Augments V_H81X Utilization in Primary Pro-B Cells

To examine potential functions of the CBE immediately downstream of V_H81X, we generated 129SV ES cells in which the 18-bp V_H81X-CBE sequence is replaced with a scrambled sequence that does not bind CTCF (Figures 1A, 1B, and S2). We introduced this mutation, referred to as "V_H81X-CBE^{scr}" into the 129SV mouse germline. V_H to DJ_H recombination occurs in progenitor (pro) B cells in the bone marrow (BM), in which overall V_H utilization frequency provides an index of relative rearrangement frequency (Lin et al., 2016; Bolland et al., 2016). To quantify utilization of each of the 100 s of distinct V_Hs across the 129SV mouse *Igh* locus in B220$^+$CD43^{high}IgM$^-$ BM pro-B cells, we employed highly sensitive high-throughput genome-wide translocation sequencing (HTGTS)-based V(D)J repertoire sequencing ("HTGTS-Rep-Seq") (Hu et al., 2015; Lin et al., 2016) using a J_H4-coding end primer as bait. For these analyses, we performed assays on four independent V_H81X-CBE^{scr} homozygous mutant mice (V_H81X-CBE$^{scr/scr}$ mice) and three wild-type (WT) controls. For statistical analyses, we normalized data from each library to 10,000 total VDJ_H junctions and similarly normal-ized data from other experiments described below (see STAR Methods).

V_H81X is the most highly utilized V_H in WT 129SV mouse pro-B cells being used in ~10% of total VDJ_H junctions, with V_H2-2, which lies ~10 kb immediately upstream, being the second most highly utilized at 6% of junctions (Figures 1C and 1D; Table S1). The three proximal V_Hs immediately upstream of V_H2-2 also are highly utilized with frequencies of 3%, 2.2%, and 1.6%, respectively (Figures 1C and 1D; Table S1). Even though WT pro-B cells have undergone locus contraction (Medvedovic et al., 2013), only a few of the most highly used V_Hs further upstream approach the 2%–3% utilization range and many are utilized far less frequently (Figure 1C). As we noted previously (Yancopoulos et al., 1984), the V_H5-1 pseudo-gene 5 kb downstream of V_H81X is infrequently utilized (~0.4%), despite its canonical RSS (Figures 1C and 1D; Table S1). Strikingly, in V_H81X-CBE$^{scr/scr}$ mutant

Author Manuscript Author Manuscript Author Manuscript Author Manuscript

mice, V_H81X utilization was reduced ~50-fold to 0.2% of junctions with a concomitant increase in uti-lization of V_H2-2 and next three upstream V_Hs (Figures 1C and 1D; Table S1). However, there were no significant effects on uti-lization of further upstream V_Hs or the downstream V_H5-1 (Figures 1C and 1D; Table S1). Thus, the V_H81X-CBE is required to promote V_H81X rearrangement in mouse pro-B cells; and, in its absence, utilization of the upstream V_H2-2 doubles to make it the most utilized V_H.

V_H81X-CBE Greatly Augments V_H81X to DJ_H Rearrangement in a *v-Abl* Pro-B Cell Line

To establish a cell culture model to facilitate further analyses of V_H81X-CBE function in V(D)J recombination, we first tested whether this element is required for V_H81X rearrangement in *v-Abl* transformed, *Eμ-Bcl2*-expressing pro-B cells viably arrested in the G1 cell-cycle phase by treatment with STI-571 to induce RAG expression and V(D)J recombination (Bredemeyer et al., 2006). For this purpose, we derived a *v-Abl* pro-B line that harbors an inert non-productive rearrangement of a distal V_HJ558 that deletes all proximal V_Hs and Ds on one allele and a D_HFL16.1 to J_H4 rearrangement that actively undergoes V_H to DJ_H recombination on the other allele (Figure 2A). Like an ATM-deficient DJ_H-rearranged *v-Abl* pro-B line (Hu et al., 2015), the D_HFL16.1J_H4 *v-Abl* pro-B line predominantly rearranges the most proximal V_Hs with only low level distal V_H rearrangement due to lack of *Igh* locus contraction in *v-Abl* lines (Figure S3A). We also employed a Cas9/gRNA approach to generate a derivative of the D_HFL16.1J_H4 line in which we deleted the V_H81X-CBE (referred to as "V_H81X-CBE^{del}" mutation) on the DJ_H allele (Figure 2B).

We analyzed three separate HTGTS-Rep-seq libraries from both parent and V_H81X-CBE^{del} D_HFL16.1J_H4 *v-Abl* pro-B lines. These analyses revealed that V_H81X is utilized in ~45% of VDJ_H rearrangements in the parent line, but in only ~0.5% of VDJ_H rearrangements in the V_H81X-CBE^{del} line, representing a 100-fold decrease (Figures 2C and S3A; Table S1). Likewise, in V_H81X-CBE^{del} D_HFL16.1J_H4 *v-Abl* cells, we observed corresponding increases in utilization of the four V_Hs upstream of V_H81X with relative utilization patterns similar to those observed in V_H81X-CBE$^{scr/scr}$ BM pro-B cells and no change in utilization of the downstream V_H5-1 (Figure 2C; Table S1). Based on these findings, we conclude that the various effects of V_H81X-CBE^{del} mutation on utilization of V_H81X and upstream neighboring proximal V_Hs are essentially identical in developing mouse pro-B cells and the D_HFL16.1J_H4 *v-Abl* pro-B cell line. Therefore, we employed this *v-Abl* pro-B line to further extend these studies and address mechanism.

V_H81X-CBE Mutation Does Not Impair V_H RSS Functionality for V(D)J Recombination

Sequencing V_H81X-CBE scrambled and deletion mutations in genomic DNA confirmed that both left the V_H81X-RSS intact. Yet, the effect of V_H81X-CBE mutations is nearly as profound and specific as expected for mutation of an RSS. To confirm that basic V_H81X-RSS functions were intact subsequent to CBE deletion, we used a Cas9/gRNA approach to delete the ~101 kb sequence downstream of the V_H81X-RSS in both D_H FL16.1J_H4 and V_H81X-CBE^{del} D_HFL16.1J_H4 *v-Abl* cells, thereby positioning V_H81X and its canonical RSS ~700 bp upstream of the DJ_HRC in both lines (Figure 2D). This large intergenic deletion mutation (referred to as "Intergenic^{del}"), which removes IGCR1 and V_H5-1, led to a

Author Manuscript Author Manuscript Author Manuscript Author Manuscript

30-fold increase in overall V_H to DJ_H joining levels in both the $D_HFL16.1J_H4$ and V_H81X-CBE^{del} $D_HFL16.1J_H4$ *v-Abl* lines (Table S2). Comparative HTGTS-Rep-seq analyses of multiple libraries from $Intergenic^{del}$ and $Intergenic^{del}$ V_H81X-CBE^{del} $D_HFL16.1J_H4$ *v-Abl* lines demonstrated that 60% of the overall increase in VDJ_H junctions in both lines involved V_H81X and that the remainder was contributed by proximal V_Hs just upstream (Figures 2E and S3B). Indeed, V_H to DJ_H rearrangement levels and patterns in the parental and V_H81X-CBE^{del} *v-Abl* lines harboring the large intergenic deletion were essentially indistinguishable (Figures 2E and S3B; Table S1). Thus, elimination of the V_H81X-CBE does not alter ability of V_H81X to undergo robust V(D)J recombination when V_H81X is positioned near the DJ_HRC, indicating that the V_H81X-CBE V(D)J recombination function is manifested at a different level than RSS-dependent RAG cleavage.

The V_H81X-CBE Mediates Robust V_H81X Rearrangement when Inverted

Several studies indicated that CBE orientation is critical for its function as a loop domain anchor (Rao et al., 2014; Sanborn et al., 2015), as well as for mediating enhancer-promoter interactions (Guo et al., 2015; de Wit et al., 2015) and regulating alternative splicing (Ruiz-Velasco et al., 2017). Convergent V_H-CBE orientation with respect to IGCR1-CBE1 and the 3′CBEs suggested that such organization may be important for V(D)J recombination regulation (Guo et al., 2011; Lin et al., 2015; Benner et al., 2015; Aiden and Casellas, 2015; Proudhon et al., 2015). To test this notion, we used a Cas9/gRNA approach to invert a 40-bp sequence encompassing V_H81X-CBE in the $D_HFL16.1J_H4$ *v-Abl* line to generate "V_H81X-CBE^{inv}" lines (Figure 2F). Comparative HTGTS-Rep-seq analyses of multiple libraries from parent and V_H81X-CBE^{inv} lines demonstrated that inversion of the V_H81X-CBE resulted in only an ~2-fold decrease in V_H81X utilization (Figures 2G and S3C; Table S1), as compared to the 100-fold reduction observed upon V_H81X-CBE deletion (Figure 2C; Table S1). Thus, the V_H81X-CBE in inverted orientation supports reduced, but still robust, V_H81X utilization.

V_H81X-CBE Promotes Interaction with the DJ_HnRC

To examine V_H81X-CBE interactions with other *Igh* regions, we developed an HTGTS-based methodology that provides high-resolution and reproducible interaction profiles of a bait locale of interest with unknown (prey) interacting sequences across *Igh* (Figure 3A). For this method, termed 3C-HTGTS, we prepare a 3C library (Dekker et al., 2002) with a 4-bp cutting restriction endonuclease and, after the sonication step, employ linear amplification-mediated-HTGTS (Frock et al., 2015; Hu et al., 2016) to complete and analyze the libraries (see STAR Methods). For our purposes, 3C-HTGTS substitutes well for prior 4C-related approaches (Denker and de Laat, 2016). In this regard, use of linear amplification to enrich for ligated products allows 3C-HTGTS to generate highly sensitive and specific interaction profiles for widely separated bait and prey sequences (Figure 3C). As all pro-B line *Igh* chromatin interaction experiments must be done in the context of RAG-deficiency to avoid confounding effects of ongoing V(D)J recombination, we used a Cas9/gRNA approach to derive RAG2-deficient derivatives of the various *v-Abl* lines.

To identify interaction partners of V_H81X, we performed 3C-HTGTS on RAG2-deficient derivatives of control, V_H81X-CBE^{del}, and V_H81X-CBE^{inv} $D_HFL16.1J_H4$ *v-Abl* lines using

Author Manuscript Author Manuscript Author Manuscript Author Manuscript

V_H81X as bait (Figure 3B). In control RAG2-deficient $D_HFL16.1J_H4$ *v-Abl* cells, V_H81X reproducibly interacts specifically with a region 100 kb downstream that spans IGCR1 and the closely linked (3 kb downstream) DJ_HnRC locale, as well as with a region 300 kb downstream containing the 3′ *Igh* CBEs (Figure 3C). Both of these interactions are dependent on the V_H81X-CBE, as they are essentially absent in V_H81X-CBE^{del} RAG2-deficient $D_HFL16.1J_H4$ *v-Abl* cells (Figure 3C). However, 3C-HTGTS analyses of the V_H81X-CBE^{inv} RAG2-deficient $D_HFL16.1J_H4$ *v-Abl* cells revealed significant V_H81X interactions with IGCR1/DJ_HnRC and 3′CBEs, albeit at moderately reduced levels compared to those of RAG2-deficient $D_HFL16.1J_H4$ control *v-Abl* cells (Figure 3C). Thus, levels of V_H81X interactions with IGCR1/DJ_HnRC locale and 3′CBEs in V_H81X-CBE inversion and deletion mutants reflect V_H81X utilization in these mutants relative to the parental $D_HFL16.1J_H4$ *v-Abl* lines, implying a potential mechanistic relationship between these interactions and V_H81X utilization.

V(D)J Recombination of V_H2-2 Is Critically Dependent on Its Flanking CBE

To test the function of an additional V_H-associated CBE, we generated "V_H2-2-CBE^{scr}" $D_HFL16.1J_H4$ *v-Abl* lines in which the CBE just downstream of V_H2-2 was replaced with a scrambled sequence that does not bind CTCF (Figure 4A). Comparative analyses of multiple HTGTS-Rep-seq libraries from the parental versus V_H2-2-CBE^{scr} mutant $D_HFL16.1J_H4$ lines demonstrated that the V_H2-2-CBE-scrambled mutation reduced V_H2-2 utilization nearly 100-fold in the V_H2-2-CBE^{scr} line (Figures 4B and S4A; Table S1). In addition, the V_H2-2-CBE^{scr} mutation led to increased utilization of the three V_Hs immediately upstream of V_H2-2, but had no effect on utilization of the downstream V_H81X and the V_H5-1 pseudo-V_H (Figure 4B). 3C-HTGTS assays performed on RAG2-deficient parental and V_H2-2-CBE^{scr} $D_HFL16.1J_H4$ *v-Abl* lines showed that V_H2-2, like V_H81X, signifi-cantly interacts with the IGCR1/DJ_HnRC locale and the 3′CBEs in a V_H2-2-CBE-dependent manner (Figures 4C, 4D, and S4B). Thus, the various effects of V_H2-2-CBE^{scr} mutation on V_H2-2 utilization, utilization of neighboring V_Hs, and long-range interactions with downstream *Igh* IGCR1/DJ_HnRC locale corresponds well with those associated with deletion of the V_H81X-CBE.

CBE-Dependent V_H81X Dominance without IGCR1 Implicates RAG Chromatin Tracking

IGCR1 deletion results in tremendous over-utilization of proximal V_Hs, most dramatically V_H81X, in association with RAG linear exploration of sequences upstream of IGCR1 via some form of tracking (Hu et al., 2015). To test whether the V_H81X-CBE contributes to the immense over-utilization of V_H81X in the context of IGCR1 deletion and RAG tracking, we generated IGCR1-deleted ("IGCR1^{del}") $D_HFL16.1J_H4$ *v-Abl* cells with or without the V_H81X-CBE^{del} mutation (Figure 5A). As expected, IGCR1 deletion led to a 30-fold increase in overall V_H to DJ_H joining levels as compared to those of the $D_HFL16.1J_H4$ parent line, involving most predominantly V_H81X and to a lesser extent proximal upstream V_Hs and the downstream V_H5-1 (Figure S5A; Tables S1 and S2). Comparative analyses of multiple HTGTS-Rep-seq libraries from IGCR1^{del} versus IGCR1^{del} V_H81X-CBE^{del} $D_HFL16.1J_H4$ lines revealed more than a 100-fold decrease in V_H81X utilization in the IGCR1^{del} V_H81X-CBE^{del} line versus the IGCR1^{del} line (Figures 5B and S5B; Table S1).

Author Manuscript Author Manuscript Author Manuscript Author Manuscript

Once again, this dramatic decrease in V_H81X utilization was accompanied by increased utilization of the four V_Hs immediately upstream of V_H81X (Figure 5B; Table S1).

To identify V_H81X-CBE interaction partners in the context of IGCR1-deficiency, we performed 3C-HTGTS using V_H81X bait on RAG2-deficient $D_HFL16.1J_H4$ *v-Abl* cells that also harbored either $IGCR1^{del}$ or $IGCR1^{del}$ V_H81X-CBE^{del} mutations (Figure 5C). As described above (Figure 3C), V_H81X has signifi-cant V_H81X-CBE-dependent interactions with the lGCR1/DJ_H nRC locale and the 3′CBEs in RAG2-deficient $D_HFL16.1J_H4$ *v-Abl* cells. However, in RAG2-deficient $IGCR1^{del}$ lines, V_H81X interaction with the DJ_HnRC locale, which we can now pinpoint in the absence of IGCR1, occurs at far higher levels than its interaction with the lGCR1/DJ_HnRC locale in RAG2-deficient $D_HFL16.1J_H4$ *v-Abl* parent line, even though interactions with the 3′CBEs remain the same or are slightly decreased (Figures 5C and S5C; top and bottom zoomed-in panels). Strikingly, in RAG2-deficient $IGCR1^{del}$ V_H81X-CBE^{del} lines, V_H81X interactions with the DJ_HnRC and 3′CBEs were essentially eliminated (Figures 5C and S5C; top and bottom zoomed-in panels).

We also used iEm within the DJ_HnRC as bait to examine interactions with other *Igh* sequences in this same set of RAG2-deficient control, $IGCR1^{del}$, and $IGCR1^{del}$ V_H81X-CBE^{del} $D_HFL16.1J_H4$ *v-Abl* lines. In all three genotypes, iEm interacted with the 3′CBEs and with a region between Cg1 and Cg2b (Medvedovic et al., 2013). In the RAG2-deficient $D_HFL16.1J_H4$ control line, iEm has barely detectable interaction with proximal V_Hs (Figures 5D and S5D; top panel). However, in RAG2-deficient $IGCR1^{del}$ lines, iEm robustly interacts with V_H81X and, at decreasing levels, with the upstream V_H2-2 and V_H5-4. In the RAG2-deficient $IGCR1^{del}$ V_H81X-CBE^{del} lines, interactions between iEm and V_H81X decreased dramatically while interactions with the immediately upstream V_H2-2 increased (Figures 5D and S5D; top and bottom zoomed-in panels). We also employed the iEm as well as another D_HQ52-J_H1 locale bait, as a distinct nRC bait for 3C-HTGTS assays in RAG2-deficient control and $IGCR1^{del/del}$ *v-Abl* lines with an unrearranged *Igh* locus and found essentially identical interaction profiles (Figure S6). Together, these 3C-HTGTS studies indicate that the impact of IGCR1 deletion on dramatically increased CBE-dependent utilization of proximal V_Hs in RAG2-sufficient WT and mutant lines directly correlates with their interaction with the DJ_HnRC in their RAG2-deficient counterparts.

Restoration of a Vestigial CBE Converts V_H5-1 into the Most Highly Rearranging V_H

Mutation of the V_H81X or V_H2-2 CBEs remarkably reduce ability of these V_Hs to be utilized for V(D)J recombination, despite retention of their normal RSSs. In this regard, the most D-proximal V_H5-1 has a canonical RSS (Figure 6A), but is infrequently rearranged in WT pro-B cells or *v-Abl* pro-B lines (Hu et al., 2015) (Figures 1C and 2C; Table S1). By employing a JASPAR sequence-based prediction, we found that V_H5-1 also is flanked downstream of its RSS by a CBE-related sequence (Figure 6A), the site of which is CpG methylated and does not bind CTCF in pro-B cells (Benner et al., 2015). To test if lack of a functional CBE causes infrequent V_H5-1 utilization, we generated $D_HFL16.1J_H4$ *v-Abl* lines (referred to as "V_H5-1-CBE^{ins}") in which 4 bps within this putative vestigial CBE were mutated to eliminate the CpG island and generate a consensus CTCF-binding element (Figure 6A). Comparative analyses of multiple HTGTS-Rep-seq libraries from the parental

Author Manuscript Author Manuscript Author Manuscript Author Manuscript

and V_H5-1-CBE^{ins} D_HFL16.1J_H4 lines demonstrated that generation of V_H5-1-CBE resulted in over a 20-fold increase in V_H5-1 utilization, converting it into the most highly utilized V_H (Figures 6B and S4C; Table S1). Notably, this gain of function V_H5-1-CBE^{ins} mutation also decreased utilization of the immediately upstream V_H81X and the next four upstream V_Hs, with their reduced utilization levels corresponding linearly with increasing distance upstream (Figure 6B). Strikingly, 3C-HTGTS studies on RAG2-deficient V_H5-1-CBE^{ins} lines demonstrated that restoration of the V_H5-1-CBE also promoted significant gain of function interactions of V_H5-1 with the IGCR1/DJ_HnRC locale and 3′CBEs (Figures 6C, 6D, and S4D), further supporting direct links between V_H recombination potential and these interactions. Finally, we deleted IGCR1 in the V_H5-1-CBE^{ins} line, which led to an 60-fold increase in V_H5-1 utilization with dramatically decreased utilization of V_H81X and other upstream proximal V_Hs (Figures S7A and S7B). Likewise, in 3C-HTGTS experiments V_H5-1 gained dramatically increased interactions with the DJ_HnRC as viewed from an iEm bait (Figure S7C).

DISCUSSION

Proximal V_H-CBEs Enhance V(D)J Recombination Potential of Associated V_Hs

We report a major role for V_H-associated CBEs in V(D)J recombination. Thus, V(D)J recombination potential of V_H81X is dramatically enhanced in both primary pro-B cells in mice and in *v-Abl* pro-B lines by its associated CBE. Likewise, V(D)J recombination potential of the upstream V_H2-2 is similarly enhanced by its associated CBE. Decades ago, we hypothe-sized one dimensional “recombinase scanning” as a possible mechanism for preferential proximal V_H utilization, but noted that there must be an additional determinant based on low level V_H5-1 pseudo-V_H utilization despite its most proximal location downstream of V_H81X and consensus RSS (Yancopoulos et al., 1984). We now identify this additional determinant as a CBE by converting the “vestigial” CBE downstream of V_H5-1 into a functional CBE and, thereby, rendering it the most frequently rearranged V_H. However, the V_H81X-CBE was not required for robust V_H81X rearrangement when it was placed linearly adjacent to the DJ_HRC, indicating V_H-CBE function is distinct from that of RSSs. To further assess the mechanism by which proximal V_H-CBEs enhance V(D)J recombination potential, we developed the highly sensitive 3C-HTGTS chromatin interaction method. Effects of various tested loss and gain of function CBE mutations on V(D)J recombination potential of the 3 proximal V_Hs were mirrored by effects on their interactions with the DJ_HnRC. This relationship was most striking in the context of IGCR1 deletion, which leads to both dramatically increased V_H81X utilization and dramatically increased V_H81X interaction with the DJ_HnRC, with both increases being dependent on the V_H81X-CBE. Thus, proximal V_H-CBEs increase V(D)J recombination potential by increasing the frequency with which their associated V_Hs interact with the DJ_HRC.

V_H-CBEs Mediate RSS Accessibility during RAG Chromatin Scanning

RAG tracking in the absence of IGCR1 proceeds upstream to the most proximal V_Hs, resulting in their increased rearrangement to DJ_H intermediates (Hu et al., 2015). This dominant increase in V_H81X rearrangement during tracking in the absence of IGCR1 is V_H81X-CBE-dependent and associated with CBE-mediated DJ_H RC interactions. The

Author Manuscript Author Manuscript Author Manuscript Author Manuscript

imprint of linear tracking on proximal V_H utilization in the absence of IGCR1 goes beyond V_H81X. Thus, in *v-Abl* pro-B lines, where tracking effects are more pronounced in the absence of locus contraction, the three V_Hs just upstream of V_H81X also show markedly increased utilization with relative utilization decreasing with upstream distance. Likewise, while V_H81X utilization plummets in V_H81X-CBE^{del} *v-Abl* cells lacking IGCR1, utilization of the upstream V_H2-2 becomes dominant and that of the three upstream V_Hs again increases with levels inversely related to upstream distance. Also consistent with linear tracking, utilization of the most downstream CBE-less V_H5-1 with a restored CBE increases substantially in the absence of IGCR1 becoming dominant even over V_H81X. Relative V_H utilization patterns during RAG upstream tracking in the absence of IGCR1 correlate well with proximal V_H interactions with the DJ_HnRC. Together, these findings indicate that RAG scans chromatin, rather than DNA *per se*, allowing this process to be better described as linear RAG chromatin scanning; and they further indicate that proximal V_H-CBEs promote over-utilization of associated V_Hs via a chromatin accessibility-enhancing function. The mechanism of this accessibility function likely involves CBE-mediated prolonged interaction of the V_H with the DJ_HRC. We find that long-range interactions critical to RAG chromatin scanning do not require a functional RAG complex. Thus, RAG bound to the DJ_HRC may harness a more general cellular mechanism operating within the *Igh* locus, such as cohesin-mediated chromatin loop extrusion, to scan distal sequences.

RAG Chromatin Scanning Shares Features with Chromatin Loop Extrusion

Inserting RSS pairs to generate ectopic “RCs” in various random genomic sites revealed orientation-specific linear RAG chromatin scanning within chromosome loop domains bounded by convergent CBE anchors, suggesting cohesin involvement (Hu et al., 2015). Features of RAG scanning overlap with those of cohesin-mediated loop extrusion (Dixon et al., 2016; Dekker and Mirny, 2016). Cohesin rings extrude chromatin loops that become progressively larger, bringing distal chromosomal regions into physical proximity in a linear fashion and having the potential to increase contact frequencies between loop anchors and sequences across extrusion domains (Fudenberg et al., 2016; Rao et al., 2017; Sanborn et al., 2015; Schwarzer et al., 2017). In this regard, CBEs bound by CTCF act as strong loop anchors and impede extrusion (Nichols and Corces, 2015; Fudenberg et al., 2016; Nora et al., 2017). Overlaps between loop extrusion and RAG scanning suggest that scanning may be driven by chromatin extrusion past a RAG-containing “RC anchor” (Figure 7). While convergent CBE anchors substantially block extrusion, other chromatin structures, such as enhancers, can impede extrusion (Dekker and Mirny, 2016). Thus, based on interactions in pro-B cells (Guo et al., 2011; Medvedovic et al., 2013; this study), IGCR1 and the J_HRC may act as upstream and downstream barriers to loop extrusion-mediated RAG scanning during D to J_H recombination. Deletion of IGCR1 would eliminate the upstream barrier and extend extrusion into proximal V_Hs, allowing V_H CTCF/cohesin-bound CBE interactions with the downstream RC extrusion anchor that increase accessibility of associated V_Hs. While V_H-CBEs increase RC interaction frequencies, they do not create absolute boundaries, as RAG scanning can extend past them at decreased levels to immediately upstream V_Hs. In contrast to certain CBE-mediated looping and regulatory processes (Sanborn et al., 2015; Guo et al., 2015; de Wit et al., 2015), V_H81X-CBE function during RAG scanning is moderately enhanced by, but not strictly dependent on, convergent

Author Manuscript Author Manuscript Author Manuscript Author Manuscript

orientation, likely due to stronger interactions in convergent orientation. Finally, proximal V_H-CBEs, DJ_HRC and 3′CBEs all interact suggesting 3′CBEs may contribute to V_H-DJ_HRC interactions. If so, deleting all 3′CBEs may influence *Igh* V(D)J recombination more than deleting a subset (Volpi et al., 2012).

Contribution of RAG Scanning to Proximal V_H Usage in the Presence of IGCR1

After *Igh* locus contraction brings distal V_Hs into closer proximity of the DJ_HRC, they become directly associated with the RC via subsequent diffusion-related mechanisms (Lucas et al., 2014). Notably, however, utilization of the very most proximal V_Hs does not require locus contraction (Fuxa et al., 2004). In this regard, primary locus-contracted pro-B cells utilize V_H81X and V_H2-2 more frequently than more distal V_Hs. Likewise, in V_H81X-CBE mutant primary pro-B cells utilization of the immediately upstream V_H2-2 increases dramatically with utilization of the next two upstream V_Hs increasing to levels higher than those of more distal V_Hs. In *v-Abl* pro-B cells, which lack *Igh* contraction but have intact IGCR1, over-utilization of V_H81X and the four immediately upstream V_Hs have a distance-dependent utilization pattern reminiscent of that when IGCR1 is inactivated. Likewise, deletion of the V_H2-2-CBE increases relative utilization of upstream V_Hs, again with the same distance-related pattern, but has no effect on downstream V_H81X utilization. Finally, ectopic introduction of an immediately downstream CBE renders proximal V_H5-1 the most highly utilized V_H, while, correspondingly, greatly dampening utilization of upstream V_Hs. Together, these findings indicate that the relatively high recombination potential of very most proximal functional V_Hs, even in normal, locus contracted pro-B cells, results from low level RAG chromatin scanning from the DJ_HRC into the proximal V_H domain in the presence of IGCR1 CBEs. Beyond these proximal V_Hs, RAG linear scanning upstream of the DJ_HRC appears to have little, if any, impact, even in the absence of IGCR1; likely because dominant utilization of proximal V_Hs first encountered obviates most RAG scanning upstream.

Potential Roles of CBEs and RAG Scanning in Distal V_H Recombination

Nearly all functional mouse V_Hs have CBEs directly adjacent or within several kb (Figure S1). In this regard, more distal V_H-CBEs likely have V(D)J recombination functions related to those we have elucidated for CBEs of the very most proximal V_Hs. The V_H portion of *Igh* comprises proximal, middle, J558 and distal J558/3609 V_H regions with different chromatin and transcriptional properties (Choi et al., 2013; Bolland et al., 2016) (Figure S1A). The proximal and middle regions largely have repressive as opposed to active chromatin marks; and V_Hs within them, including V_H81X, show little or no germline transcription. Correspondingly, the majority of proximal/middle V_Hs, in addition to the few accessible to RAG linear scanning, have CBEs adjacent to their RSSs that may stabilize diffusion-mediated interactions with the DJ_HRC to promote accessibility (Figures S1B, S1C, and 7A). Notably, the J558 and, particularly, the distal J558/3609 regions have accessible chromatin marks and regions of transcription. In contrast to proximal V_Hs, few distal V_Hs are directly associated with a CBE, but most have CBEs within 10 kb and often much closer (Figures S1D and S1E). Such CBEs in distal domains still may enhance diffusion-mediated interactions with the DJ_HRC directly or in association with other interacting sequences such as IGCR1 or the 3′CBEs. Interactions with CBEs not directly associated with V_Hs also

Author Manuscript Author Manuscript Author Manuscript Author Manuscript

could provide anchors for loop extrusion of the locally accessible distal V_Hs past the RC (Figures 7D–7F). Thereby, distal V_Hs may be utilized without an immediately adjacent CBE. Other antigen receptor loci in mouse and humans also have large numbers of CBEs (Proudhon et al., 2015; Bolland et al., 2016), including some in *Igκ* and *Tcr*α/δ that play IGCR1-like functions (Xiang et al., 2014; Chen et al., 2015). RAG scanning in TCRδ also is restricted to CBE-anchored loop domains (Zhao et al., 2016). Similar to the proximal and distal *Igh*, differing V domain CBE organizations among antigen receptor loci also might function in the context of RAG scanning/loop extrusion. Why different antigen receptor loci domains evolved different CBE organizational solutions to regulate V_H usage remains an interesting question.

STAR★ METHODS

Detailed methods are provided in the online version of this paper and include the following:

KEY RESOURCES TABLE

REAGENT or RESOURCE	SOURCE	IDENTIFIER
Antibodies		
Rabbit polyclonal anti-CTCF	EMD Millipore	Cat#07-729
APC anti-B220	eBioscience	Cat#18-0452-83
FITC anti-IgM	eBioscience	Cat#11-5790-81
PE anti-CD43	BD PharMingen	Cat#553271
Bacterial and Virus Strains		
DH5a Competent Cells	Thermo Fisher Scientific	Cat#18265017
pMSCV-*v-Abl* retrovirus	Bredemeyer et al., 2006	N/A
Chemicals, Peptides, and Recombinant Proteins		
G418 Sulfate	Thermo Fisher Scientific	Cat#11811031
*Not*I	NEB	Cat#R0189
*Xba*I	NEB	Cat#R0145
*Eco*RV	NEB	Cat#R0195
*Nla*III	NEB	Cat#R0125
*Mse*I	NEB	Cat#R0525
Red Blood Cell Lysing Buffer Hybri-Max	Sigma-Aldrich	Cat#R7757
STI-571	Novartis	N/A
Dynabeads MyOne Streptavidin C1	Thermo Fisher Scientific	Cat#65001
Phusion High-Fidelity DNA Polymerase	NEB	Cat#M0530L
Protease inhibitors	Roche	Cat#11836153001
T4 DNA ligase	Promega	Cat#M1804
Proteinase K	Roche	Cat#03115852001
RNase A	Invitrogen	Cat#8003089
Critical Commercial Assays		

Author Manuscript Author Manuscript Author Manuscript Author Manuscript

REAGENT or RESOURCE	SOURCE	IDENTIFIER
LightShift Chemiluminescent EMSA kit	Thermo Fisher Scientific	Cat#20148
MiSeq Reagent Kit v3 (600 cycle)	Illumina	Cat#MS-102-3003
MiSeq Reagent Kit v2 (500 cycle)	Illumina	Cat#MS-102-2003
PhiX Control v3 Kit	Illumina	Cat#FC-110-3001
Deposited Data		
Raw data of pro-B HTGTS-Rep-Seq	This paper	GEO: GSExxxxx
Raw data of D_HFL16.1J_H4 HTGTS-Rep-Seq	This paper	GEO: GSExxxxx
Raw data of 3C-HTGTS	This paper	GEO: GSExxxxx
Raw data of CTCF ChIP-seq	Choi et al., 2013	GEO: GSE47766
Raw data of Rad21 ChIP-seq	Choi et al., 2013	GEO: GSE47766
Raw data of Pax5 ChIP-seq	Revilla-I-Domingo et al., 2012	GEO: GSE38046
Raw data of YY1 ChIP-seq	Medvedovic et al., 2013	GEO: GSE43008
Experimental Models: Cell Lines		
129SV TC1 embryonic stem (ES) cells	Guo et al., 2011	N/A
D_HFL16.1J_H4 *Eμ-Bcl2 v-Abl* pro-B line	This paper	N/A
D_HFL16.1J_H4 *Eμ-Bcl2 Rag*$^{-/-}$ *v-Abl* pro-B line	This paper	N/A
D_HFL16.1J_H4 *Eμ-Bcl2* V_H81X-CBE^{del} *v-Abl* pro-B line	This paper	N/A
D_HFL16.1J_H4 *Eμ-Bcl2* V_H81X-CBE^{del} *Rag2*$^{-/-}$ *v-Abl* pro-B line	This paper	N/A
D_HFL16.1J_H4 *Eμ-Bcl2* Intergenic^{del} *v-Abl* pro-B line	This paper	N/A
D_HFL16.1J_H4 *Eμ-Bcl2* Intergenic^{del} V_H81X-CBE^{del} *v-Abl* pro-B line	This paper	N/A
D_HFL16.1J_H4 *Eμ-Bcl2* V_H81X-CBE^{inv} *v-Abl* pro-B line	This paper	N/A
D_HFL16.1J_H4 *Eμ-Bcl2* V_H81X-CBE^{inv} *Rag2*$^{-/-}$ *v-Abl* pro-B line	This paper	N/A
D_HFL16.1J_H4 *Eμ-Bcl2* V_H2-2-CBE^{scr} *v-Abl* pro-B line	This paper	N/A
D_HFL16.1J_H4 *Eμ-Bcl2* V_H2-2-CBE^{scr} *Rag2*$^{-/-}$ *v-Abl* pro-B line	This paper	N/A
D_HFL16.1J_H4 *Eμ-Bcl2* V_H5-1-CBE^{ins} *v-Abl* pro-B line	This paper	N/A
D_HFL16.1J_H4 *Eμ-Bcl2* V_H5-1-CBE^{ins} *Rag2*$^{-/-}$ *v-Abl* pro-B line	This paper	N/A
D_HFL16.1J_H4 *Eμ-Bcl2* IGCR1^{del} *v-Abl* pro-B line	This paper	N/A
D_HFL16.1J_H4 *Eμ-Bcl2* IGCR1^{del} *Rag2*$^{-/-}$ *v-Abl* pro-B line	This paper	N/A
D_HFL16.1J_H4 *Eμ-Bcl2* IGCR1^{del} V_H81X-CBE^{del} *v-Abl* pro-B line	This paper	N/A
D_HFL16.1J_H4 *Eμ-Bcl2* IGCR1^{del}; V_H81X-CBE^{del} *Rag2*$^{-/-}$ *v-Abl* pro-B line	This paper	N/A

Author Manuscript Author Manuscript Author Manuscript Author Manuscript

REAGENT or RESOURCE	SOURCE	IDENTIFIER
$D_HFL16.1J_H4$ *Eμ-Bcl2* $IGCR1^{del}$ V_H5-1-CBE^{ins} *v-Abl* pro-B line	This paper	N/A
$D_HFL16.1J_H4$ *Eμ-Bcl2* $IGCR1^{del}$; V_H5-1-CBE^{ins} $Rag2^{-/-}$ *v-Abl* pro-B line	This paper	N/A
$Rag2^{-/-}$ *v-Abl* pro-B line	This paper	N/A
$Rag2^{-/-}$ $IGCR1^{del/del}$ *v-Abl* pro-B line	This paper	N/A
$Rag2^{-/-}$ $IGCR1^{del/del}$ V_H81X-$CBE^{scr/scr}$ *v-Abl* pro-B line	This paper	N/A
Experimental Models: Organisms/Strains		
V_H81X-$CBE^{scr/scr}$ mice	This paper	N/A
129SVE mice	Taconic	N/A
Oligonucleotides		
Primers for targeting vector construction, Southern probes and PCR screening	This paper; Table S3	N/A
gDNAs and ssODNs for gene targeting	This paper; Table S3	N/A
Primers for HTGTS-Rep-Seq and 3C-HTGTS	This paper; Table S4	N/A
Adaptors and common primers for HTGTS	Hu et al., 2016	N/A
Recombinant DNA		
pX330-U6-Chimeric_BB-CBh-hSpCas9	Addgene	Cat#42230
pGEM-T Easy Vector	Promega	Cat#A1360
pLNTK	Guo et al., 2011	N/A
Software and Algorithms		
HTGTS pipeline	Hu et al., 2016	http://robinmeyers.github.io/transloc_pipeline/
Bowtie2 v2.2.8	Langmead and Salzberg, 2012	http://bowtie-bio.sourceforge.net/bowtie2/index.shtml
MACS (2.1.0)	Zhang et al., 2008	https://github.com/taoliu/MACS
GraphPad Prism 7.0 Software	GraphPad	https://www.graphpad.com/

CONTACT FOR REAGENT AND RESOURCE SHARING

Further information and requests for resources and reagents should be directed to and will be fulfilled by the Lead Contact, Frederick W. Alt (alt@enders.tch.harvard.edu).

EXPERIMENTAL MODEL AND SUBJECT DETAILS

Mice—A 2.2-kb 5′ homology arm encompassing the V_H81X gene segment sequence and containing an 18-bp scrambled mutation of V_H81X-CBE that abrogates CTCF binding (Figure S2A) and a 5-kb 3′ homology arm containing sequences downstream V_H81X-CBE were cloned into the pLNTK targeting vector containing a pGK-Neo^R cassette (Figure S2B). 129SV TC1 embryonic stem (ES) cells were electroporated with this targeting construct and ES clones were screened for correct targeted mutations by Southern blotting and confirmed by PCR-digestion using the strategies outlined in detail in Figures S2C–S2F. Two correctly targeted ES clones were injected for germline transmission following Cre-loxP mediated deletion of the Neo^R gene, one of which contributed to the germline yielding V_H81X-

Author Manuscript Author Manuscript Author Manuscript Author Manuscript

CBE$^{wt/scr}$ 129SV mice, which were bred to yield V_H81X-CBE$^{scr/scr}$ mice and their WT littermates that were used for analyses. As our targeting strategy to generate the V_H81X-CBE^{scr} allele also placed a *loxP* sequence 642 bp downstream of the V_H81X-CBE^{scr} mutation, we generated control mice harboring only the *loxP* insertion, without the V_H81X-CBE scramble mutation, and found that their BM pro-B cells had V_H utilization patterns that were not significantly different than those of WT (S.J., F.W.A., unpublished data). Primers used for construction of targeting vector, Southern probes and PCR screening are listed in Table S3. All animal experiments were performed under protocols approved by the Institutional Animal Care and Use Committee of Boston Children's Hospital.

Cell lines—*v-Abl* kinase transformed pro-B cell lines were derived by retroviral infection of bone marrow cells from 4-6 weeks old mice with the pMSCV-*v-Abl* retrovirus, as previously described (Bredemeyer et al., 2006). Transfected cells were cultured in RPMI medium containing 15% (v/v) FBS for two months to recover stably transformed *v-Abl* pro-B cell lines. The "D_HFL16.1J_H4" line was generated by transiently inducing RAG expression in *v-Abl* pro-B cell lines derived from *Eμ-Bcl2* transgenic mice by arresting them in G1 for 4 days by treatment with 3 μM STI-571 (Hu et al., 2015). Single cell clones were screened for V_HDJ_H and DJ_H rearrangements first by PCR using degenerate V_H and D primers together with a J_H4 primer (Guo et al., 2011) and subsequently confirmed by Southern blotting to isolate the parental D_HFL16.1J_H4 line (See Figure 2A for diagrams of the DJ_H and non-productive VDJ_H alleles in the D_HFL16.1J_H4 line).

All mutant lines analyzed in this study (except those shown in Figure S6) were derived from this D_HFL16.1J_H4 parental line or its direct derivatives by Cas9/gRNA approaches (Cong et al., 2013). The V_H81X-CBE^{del} mutant was generated by imprecise rejoining of a DSB induced by a gRNA that targets the V_H81X-CBE. The V_H81X-CBE^{inv}, V_H2-2-CBE^{scr}, and V_H5-1-CBE^{ins} lines were obtained by homologous recombination-mediated repair of targeted DNA breaks introduced by Cas9/gRNA with single-stranded DNA oligonucleotides (ssODNs) as template (Ran et al., 2013). The IGCR1 deletion mutants of the parental, V_H81X-CBE^{del} and V_H5-1-CBE^{ins} D_HFL16.1J_H4 lines were derived via a Cas9/gRNA targeting approach based on using two gRNAs specific to sites flanking the intended IGCR1 deletion. The 101-kb intergenic deletion was derived from parental and V_H81X-CBE^{del} D_HFL16.1J_H4 lines using gRNAs that target sites flanking the intended deletion. At least two independent lines were derived and analyzed for each mutation studied except for the V_H81X-CBE^{del}. However, from the same D_HFL16.1J_H4 parental line, we generated an additional line in which the V_H81X-CBE was disrupted by a random 13-bp insertion (not shown), and found that it had V_H-utilization patterns essentially identical to those of the V_H81X-CBE^{del} line. *Rag2* was deleted by the Cas9/gRNA approach mentioned above from all of the lines analyzed by 3C-HTGTS to study chromatin interactions. The *v-Abl* lines shown in Figure S6 were derived by retroviral infection of bone marrow cells (see above) from *Rag*$^{-/-}$ and *Rag*$^{-/-}$ V_H81X$^{scr/scr}$ mice, and subsequently targeted for IGCR1 deletion via the Cas9/gRNA approach. Sequences of all gRNAs and ssODNs are listed in Table S3.

Author Manuscript Author Manuscript Author Manuscript Author Manuscript

METHOD DETAILS

Bone marrow pro-B cell purification—Single cell suspensions were derived from bone marrows of 4-6 weeks old mice and incubated in Red Blood Cell Lysing Buffer (Sigma-Aldrich, #R7757) to deplete the erythrocytes. Remaining cells were stained with anti-B220-APC (eBioscience, #17-0452-83), anti-CD43-PE (BD PharMingen, #553271), and anti-IgM-FITC (eBioscience, #11-5790-81) antibodies for 30 minutes at 4 C. Excess antibodies were washed off and $B220^{+}CD43^{high}IgM^{-}$ pro-B cells were isolated (Guo et al., 2011) by FACS sorting using a BD FACSARIA III cell sorter.

HTGTS-Rep-Seq to determine V_H utilization frequencies—HTGTS-Rep-Seq was performed and data were analyzed with all duplicate junctions included in the analyses as previously described (Hu et al., 2016). Briefly, 2 mg of genomic DNA from sorted mouse primary pro-B cells or 50 mg of genomic DNA isolated from *v-Abl* lines following 4 days of G1 arrest by treatment with 3 μM STI-571, was sonicated for 25 s ON and 60 s OFF for two cycles on a Diagenode Bioruptor sonicator at low setting. Sonicated DNA was linearly amplified with a biotinylated J_H4 coding end primer that anneals downstream of the J_H4 segment. The biotin-labeled single-stranded DNA products were enriched with streptavidin C1 beads (Thermo Fisher Scientific, #65001), and 3′ ends were ligated with the bridge adaptor containing a 6-nucleotide overhang. The adaptor-ligated products were amplified by a nested J_H4 coding end primer and an adaptor-complementary primer. The products were then prepared for sequencing on Illumina MiSeq platform after tagging with the P5-I5 and P7-I7 sequences (Hu et al., 2016). Junctions were aligned to AJ851868/mm9 hybrid genome by combining all of the annotated 129SV *Igh* sequences (AJ851868) and the distal V_H sequences from the C57BL/6 background (mm9) starting from V_H8-2 as described in Lin et al. (2016). The sequence of the J_H4 coding end primer used for making HTGTS-Rep-Seq libraries is listed in Table S4. In primary pro-B cells, our assay recovers D-to-J_H4 as well as V_H-to-DJ_H4 junctions; whereas in the $D_HFL16.1J_H4$ rearranged *v-Abl* pro-B lines, we recover V_H to $D_HFL16.1J_H4$ rearrangements using the J_H4 baiting primer. In the $D_HFL16.1J_H4$ lines, this primer also amplifies across J_H4 on the pre-rearranged V_HDJ_H3 rearranged non-productive allele (Figure 2A); however, those reads are all filtered out as germline reads and are, thus, excluded from our V(D)J junction analyses.

As our experiments are done in G1-arrested cells, all *de novo* rearrangements should represent unique events. However, rearrangements at low but variable levels can occur in cycling *v-Abl* lines and can be well above background in some sub-clones (e.g., Alt et al., 1981) Therefore, after each HTGTS experiment, data were analyzed for high levels of recurrent *Igh* V(D)J junctional sequences suggestive of a pre-rearranged V(D)J rearrangement that likely occurred in cycling cells during culture. Then, if necessary, experiments were repeated on additional sub-clones that lacked evidence of obvious pre-rearrangements.

For statistical analyses, each HTGTS library plotted for comparison in a figure panel was normalized for by random selection of the number of junctions recovered from the smallest library in the comparison set. While normalization was done for statistical comparison, we note that relative V_H utilization patterns were essentially same in normalized and un-

Author Manuscript Author Manuscript Author Manuscript Author Manuscript

normalized libraries. The numbers of junctions used for normalization of IGCR1^{del} or 101-kb intergenic^{del} experiments was much higher than those shown for panels comparing WT and other mutant backgrounds due to the greatly increased levels of V_H to DJ_H junctions recovered upon IGCR1-deletion or 101-kb intergenic deletion as described in main text and shown in Figure S5A and Table S2. The numbers of junctions recovered in each replicate experiment are listed in Table S5. Data plots show average utilization frequencies ± SD.

For *v-Abl* lines, the same WT data is shown in Figures 2C, 2G, 4B, 6B and their associated supplementary figures, as all mutant lines were derived from a single WT $D_HFL16.1J_H4$ parent line. As such, several different mutants were analyzed alongside the WT control in any given experiment and the WT control was simultaneously analyzed with each mutant at least once to ensure that the WT line gave the same rearrangement pattern over the course of the entire study. Final WT averages were calculated from data collected over the course of this study. We also show the same IGCR1^{del} $D_HFL16.1J_H4$ control data in Figures 5B, S5B, S7A, and S7B, as we used the same gRNA strategy, respectively, to generate IGCR1^{del}, IGCR1^{del} V_H81X-CBE^{del}, and IGCR1^{del} V_H5-1-CBE^{ins} lines from the same common $D_HFL16.1J_H4$ ancestor line (as described above). The IGCR1^{del} data is plotted as the average of experiments done along with IGCR1^{del} V_H81X-CBE^{del} or IGCR1^{del} V_H5-1-CBE^{ins} lines.

The non-productive fraction of V_HDJ_H reads obtained from C57BL/6 pro-B cells shown in Figure S1 were extracted from data in a prior publication (Lin et al., 2016).

3C-HTGTS—3C libraries were generated as previously described (Splinter et al., 2012; Stadhouders et al., 2013). Briefly, 10 million cells were cross-linked with 2% (v/v) formaldehyde for 10’ at room temperature, followed by quenching with glycine at a final concentration of 125 mM. Cells were lysed in 50 mM Tris-HCl, pH 7.5, containing 150 mM NaCl, 5 mM EDTA, 0.5% NP-40, 1% Triton X-100 and protease inhibitors (Roche, #11836153001). Nuclei were digested with 700 units of *Nla*III (NEB, #R0125) or *Mse*I (NEB, #R0525) restriction enzyme at 37°C overnight, followed by ligation under dilute conditions at 16°C overnight. Crosslinks were reversed and samples were treated with Proteinase K (Roche, #03115852001) and RNase A (Invitrogen, #8003089) prior to DNA precipitation. The 3C libraries were sonicated for 25 s ON and 60 s OFF for two cycles on a Diagenode Bioruptor Sonicator at low setting. LAM-HTGTS libraries were then prepared and analyzed as described in “HTGTS-Rep-Seq to determine V_H utilization frequencies” section (see also Hu et al., 2016) and data was aligned to AJ851868/mm9 hybrid genome as described in Lin et al. (2016) with an additional modification in which Chr12 coordinates from 114671120 to 114734564 in the AJ851868/mm9 hybrid genome were replaced with CCCCT to incorporate the $D_HFL16.1$ to J_H4 rearrangement for aligning data obtained from the $D_HFL16.1J_H4$ rearranged *v-Abl* pro-B lines. When using the iEm bait, we also detected interactions with distal regions beyond V_H1-2P in the $D_HFL16.1J_H4$ rearranged *v-Abl* pro-B lines due to close linear juxtaposition of this region to iEm owing to the V_HDJ_H rearrangement of V_H1-2P on the non-productive allele. These interactions were not detected in the unrearranged *v-Abl* pro-B lines or primary pro-B cells as evident from data deposited in GEO database. The primers used for making 3C-HTGTS libraries are listed in Table S4. Data were plotted for comparison after normalizing junction from each experimental 3C-

Author Manuscript Author Manuscript Author Manuscript Author Manuscript

HTGTS library by random selection to the total number of genome-wide junctions recovered from the smallest library in the set of libraries being compared. However, chromosomal interaction patterns were very similar in normalized and un-normalized libraries.

Electrophoretic Mobility Shift Assay (EMSA)—EMSA was performed with oligos (shown in Figure S2A) using the LightShift Chemiluminescent EMSA kit from Thermo Fisher Scientific (Catalog #20148) as per manufacturer's protocol. 2 mg of anti-CTCF antibody from Millipore (Catalog #07-729) was used to detect super-shift.

ChIP-seq—CTCF and Rad21 ChIP-seq data were extracted from Choi et al. (2013) (GEO: GSE47766). Pax5 and YY1 ChIP-seq data was extracted from Revilla-I-Domingo et al., 2012 (GEO: GSE38046) and Medvedovic et al. (2013) (GEO: GSE43008), respectively. The ChIP-seq data were re-analyzed by aligning to mm9 and ChIP-seq peaks were called using MACS with default parameters (Zhang et al., 2008).

QUANTIFICATION AND STATISTICAL ANALYSIS

An unpaired, two-tailed Student's t test was used to determine the statistical significance of differences between samples, ns indicates $p > 0.05$, * $p \leq 0.05$, ** $p \leq 0.01$ and *** $p \leq 0.001$.

DATA AND SOFTWARE AVAILABILITY

The Gene Expression Omnibus (GEO) accession number for the datasets reported in this paper is GEO: GSE113023. Specifically, the GEO accession numbers for pro-B-HTGTS-Rep-Seq, $D_HFL16.1J_H4$-HTGTS-Rep-Seq and 3C-HTGTS datasets are GEO: GSE112781, GEO: GSE112822 and GEO: GSE113022, respectively.

Supplementary Material

Refer to Web version on PubMed Central for supplementary material.

Acknowledgments

We thank Hye-Suk Yoon and Arthur Su for contributions to preliminary analyses and Jeffrey Zurita for bioinformatics advice. This work was supported by NIH (AI020047). F.W.A. is a Howard Hughes Medical Institute Investigator. Z.B. is supported by a Cancer Research Institute Irvington Fellowship. Y.Z. is supported by a Leukemia and Lymphoma Society Special Fellow Award.

References

Aiden EL, Casellas R. Somatic rearrangement in B cells: it's (mostly) *nuclear physics*. Cell. 2015; 162:708–711. [PubMed: 26276627]

Alt F, Rosenberg N, Lewis S, Thomas E, Baltimore D. Organization and reorganization of immunoglobulin genes in A-MULV-transformed cells: rearrangement of heavy but not light chain genes. Cell. 1981; 27:381–390. [PubMed: 6277505]

Alt FW, Zhang Y, Meng FL, Guo C, Schwer B. Mechanisms of programmed DNA lesions and genomic instability in the immune system. Cell. 2013; 152:417–429. [PubMed: 23374339]

Benner C, Isoda T, Murre C. New roles for DNA cytosine modification, eRNA, anchors, and superanchors in developing B cell progenitors. Proc Natl Acad Sci USA. 2015; 112:12776–12781. [PubMed: 26417104]

Author Manuscript Author Manuscript Author Manuscript Author Manuscript

Bolland DJ, Koohy H, Wood AL, Matheson LS, Krueger F, Stubbington MJT, Baizan-Edge A, Chovanec P, Stubbs BA, Tabbada K, et al. Two mutually exclusive local chromatin states drive efficient V(D)J recombination. Cell Rep. 2016; 15:2475–2487. [PubMed: 27264181]

Bossen C, Mansson R, Murre C. Chromatin topology and the regulation of antigen receptor assembly. Annu Rev Immunol. 2012; 30:337–356. [PubMed: 22224771]

Bredemeyer AL, Sharma GG, Huang CY, Helmink BA, Walker LM, Khor KC, Nuskey B, Sullivan KE, Pandita TK, Bassing CH, Sleckman BP. ATM stabilizes DNA double-strand-break complexes during V(D)J recombination. Nature. 2006; 442:466–470. [PubMed: 16799570]

Chen L, Carico Z, Shih HY, Krangel MS. A discrete chromatin loop in the mouse Tcra-Tcrd locus shapes the TCRδ and TCRα repertoires. Nat Immunol. 2015; 16:1085–1093. [PubMed: 26258942]

Choi NM, Loguercio S, Verma-Gaur J, Degner SC, Torkamani A, Su AI, Oltz EM, Artyomov M, Feeney AJ. Deep sequencing of the murine IgH repertoire reveals complex regulation of nonrandom V gene rearrangement frequencies. J Immunol. 2013; 191:2393–2402. [PubMed: 23898036]

Cong L, Ran FA, Cox D, Lin S, Barretto R, Habib N, Hsu PD, Wu X, Jiang W, Marraffini LA, Zhang F. Multiplex genome engineering using CRISPR/Cas systems. Science. 2013; 339:819–823. [PubMed: 23287718]

de Wit E, Vos ESM, Holwerda SJB, Valdes-Quezada C, Verstegen MJAM, Teunissen H, Splinter E, Wijchers PJ, Krijger PHL, de Laat W. CTCF binding polarity determines chromatin looping. Mol Cell. 2015; 60:676–684. [PubMed: 26527277]

Degner SC, Verma-Gaur J, Wong TP, Bossen C, Iverson GM, Torkamani A, Vettermann C, Lin YC, Ju Z, Schulz D, et al. CCCTC-binding factor (CTCF) and cohesin influence the genomic architecture of the Igh locus and antisense transcription in pro-B cells. Proc Natl Acad Sci USA. 2011; 108:9566–9571. [PubMed: 21606361]

Dekker J, Mirny L. The 3D genome as moderator of chromosomal communication. Cell. 2016; 164:1110–1121. [PubMed: 26967279]

Dekker J, Rippe K, Dekker M, Kleckner N. Capturing chromosome conformation. Science. 2002; 295:1306–1311. [PubMed: 11847345]

Denker A, de Laat W. The second decade of 3C technologies: detailed insights into nuclear organization. Genes Dev. 2016; 30:1357–1382. [PubMed: 27340173]

Dixon JR, Selvaraj S, Yue F, Kim A, Li Y, Shen Y, Hu M, Liu JS, Ren B. Topological domains in mammalian genomes identified by analysis of chromatin interactions. Nature. 2012; 485:376–380. [PubMed: 22495300]

Dixon JR, Gorkin DU, Ren B. Chromatin domains: the unit of chromosome organization. Mol Cell. 2016; 62:668–680. [PubMed: 27259200]

Ebert A, Hill L, Busslinger M. Spatial regulation of V-(D)J recombination at antigen receptor loci. Adv Immunol. 2015; 128:93–121. [PubMed: 26477366]

Frock RL, Hu J, Meyers RM, Ho YJ, Kii E, Alt FW. Genome-wide detection of DNA double-stranded breaks induced by engineered nucleases. Nat Biotechnol. 2015; 33:179–186. [PubMed: 25503383]

Fudenberg G, Imakaev M, Lu C, Goloborodko A, Abdennur N, Mirny LA. Formation of chromosomal domains by loop extrusion. Cell Rep. 2016; 15:2038–2049. [PubMed: 27210764]

Fuxa M, Skok J, Souabni A, Salvagiotto G, Roldan E, Busslinger M. Pax5 induces V-to-DJ rearrangements and locus contraction of the immunoglobulin heavy-chain gene. Genes Dev. 2004; 18:411–422. [PubMed: 15004008]

Guo C, Yoon HS, Franklin A, Jain S, Ebert A, Cheng HL, Hansen E, Despo O, Bossen C, Vettermann C, et al. CTCF-binding elements mediate control of V(D)J recombination. Nature. 2011; 477:424–430. [PubMed: 21909113]

Guo Y, Xu Q, Canzio D, Shou J, Li J, Gorkin DU, Jung I, Wu H, Zhai Y, Tang Y, et al. CRISPR inversion of CTCF sites alters genome topology and enhancer/promoter function. Cell. 2015; 162:900–910. [PubMed: 26276636]

Hnisz D, Day DS, Young RA. Insulated neighborhoods: structural and functional units of mammalian gene control. Cell. 2016; 167:1188–1200. [PubMed: 27863240]

Hu J, Zhang Y, Zhao L, Frock RL, Du Z, Meyers RM, Meng FL, Schatz DG, Alt FW. Chromosomal loop domains direct the recombination of antigen receptor genes. Cell. 2015; 163:947–959. [PubMed: 26593423]

Author Manuscript Author Manuscript Author Manuscript Author Manuscript

Hu J, Meyers RM, Dong J, Panchakshari RA, Alt FW, Frock RL. Detecting DNA double-stranded breaks in mammalian genomes by linear amplification-mediated high-throughput genome-wide translocation sequencing. Nat Protoc. 2016; 11:853–871. [PubMed: 27031497]

Kim MS, Lapkouski M, Yang W, Gellert M. Crystal structure of the V(D)J recombinase RAG1-RAG2. Nature. 2015; 518:507–511. [PubMed: 25707801]

Langmead B, Salzberg SL. Fast gapped-read alignment with Bowtie 2. Nat Methods. 2012; 9:357–359. [PubMed: 22388286]

Lin SG, Guo C, Su A, Zhang Y, Alt FW. CTCF-binding elements 1 and 2 in the Igh intergenic control region cooperatively regulate V(D) J recombination. Proc Natl Acad Sci USA. 2015; 112:1815–1820. [PubMed: 25624508]

Lin SG, Ba Z, Du Z, Zhang Y, Hu J, Alt FW. Highly sensitive and unbiased approach for elucidating antibody repertoires. Proc Natl Acad Sci USA. 2016; 113:7846–7851. [PubMed: 27354528]

Lucas JS, Zhang Y, Dudko OK, Murre C. 3D trajectories adopted by coding and regulatory DNA elements: first-passage times for genomic interactions. Cell. 2014; 158:339–352. [PubMed: 24998931]

Medvedovic J, Ebert A, Tagoh H, Tamir IM, Schwickert TA, Novatch-kova M, Sun Q, Huis In 't Veld PJ, Guo C, Yoon HS, et al. Flexible long-range loops in the VH gene region of the Igh locus facilitate the generation of a diverse antibody repertoire. Immunity. 2013; 39:229–244. [PubMed: 23973221]

Merkenschlager M, Nora EP. CTCF and cohesin in genome folding and transcriptional gene regulation. Annu Rev Genomics Hum Genet. 2016; 17:17–43. [PubMed: 27089971]

Nichols MH, Corces VG. A CTCF code for 3D genome architecture. Cell. 2015; 162:703–705. [PubMed: 26276625]

Nora EP, Lajoie BR, Schulz EG, Giorgetti L, Okamoto I, Servant N, Piolot T, van Berkum NL, Meisig J, Sedat J, et al. Spatial partitioning of the regulatory landscape of the X-inactivation centre. Nature. 2012; 485:381–385. [PubMed: 22495304]

Nora EP, Goloborodko A, Valton AL, Gibcus JH, Uebersohn A, Abdennur N, Dekker J, Mirny LA, Bruneau BG. Targeted degradation of CTCF decouples local insulation of chromosome domains from genomic compartmentalization. Cell. 2017; 169:930–944. [PubMed: 28525758]

Phillips-Cremins JE, Sauria MEG, Sanyal A, Gerasimova TI, Lajoie BR, Bell JSK, Ong CT, Hookway TA, Guo C, Sun Y, et al. Architectural protein subclasses shape 3D organization of genomes during lineage commitment. Cell. 2013; 153:1281–1295. [PubMed: 23706625]

Proudhon C, Hao B, Raviram R, Chaumeil J, Skok JA. Long-range regulation of V(D)J recombination. Adv Immunol. 2015; 128:123–182. [PubMed: 26477367]

Ran FA, Hsu PD, Wright J, Agarwala V, Scott DA, Zhang F. Genome engineering using the CRISPR-Cas9 system. Nat Protoc. 2013; 8:2281–2308. [PubMed: 24157548]

Rao SSP, Huntley MH, Durand NC, Stamenova EK, Bochkov ID, Robinson JT, Sanborn AL, Machol I, Omer AD, Lander ES, Aiden EL. A 3D map of the human genome at kilobase resolution reveals principles of chromatin looping. Cell. 2014; 159:1665–1680. [PubMed: 25497547]

Rao SSP, Huang SC, Glenn St Hilaire B, Engreitz JM, Perez EM, Kieffer-Kwon KR, Sanborn AL, Johnstone SE, Bascom GD, Bochkov ID, et al. Cohesin loss eliminates all loop domains. Cell. 2017; 171:305–320. [PubMed: 28985562]

Revilla-I-Domingo R, Bilic I, Vilagos B, Tagoh H, Ebert A, Tamir IM, Smeenk L, Trupke J, Sommer A, Jaritz M, Busslinger M. The B-cell identity factor Pax5 regulates distinct transcriptional programmes in early and late B lymphopoiesis. EMBO J. 2012; 31:3130–3146. [PubMed: 22669466]

Ru H, Chambers MG, Fu TM, Tong AB, Liao M, Wu H. Molecular mechanism of V(D)J recombination from synaptic RAG1-RAG2 complex structures. Cell. 2015; 163:1138–1152. [PubMed: 26548953]

Ruiz-Velasco M, Kumar M, Lai MC, Bhat P, Solis-Pinson AB, Reyes A, Kleinsorg S, Noh KM, Gibson TJ, Zaugg JB. CTCF-mediated chromatin loops between promoter and gene body regulate alternative splicing across individuals. Cell Syst. 2017; 5:628–637. [PubMed: 29199022]

Sanborn AL, Rao SSP, Huang SC, Durand NC, Huntley MH, Jewett AI, Bochkov ID, Chinnappan D, Cutkosky A, Li J, et al. Chromatin extrusion explains key features of loop and domain formation

Author Manuscript Author Manuscript Author Manuscript Author Manuscript

in wild-type and engineered genomes. Proc Natl Acad Sci USA. 2015; 112:E6456–E6465. [PubMed: 26499245]

Schwarzer W, Abdennur N, Goloborodko A, Pekowska A, Fudenberg G, Loe-Mie Y, Fonseca NA, Huber W, H Haering C, Mirny L, Spitz F. Two independent modes of chromatin organization revealed by cohesin removal. Nature. 2017; 551:51–56. [PubMed: 29094699]

Splinter E, de Wit E, van de Werken HJG, Klous P, de Laat W. Determining long-range chromatin interactions for selected genomic sites using 4C-seq technology: from fixation to computation. Methods. 2012; 58:221–230. [PubMed: 22609568]

Stadhouders R, Kolovos P, Brouwer R, Zuin J, van den Heuvel A, Kockx C, Palstra RJ, Wendt KS, Grosveld F, van Ijcken W, Soler E. Multiplexed chromosome conformation capture sequencing for rapid genome-scale high-resolution detection of long-range chromatin interactions. Nat Protoc. 2013; 8:509–524. [PubMed: 23411633]

Teng G, Schatz DG. Regulation and evolution of the RAG recombinase. Adv Immunol. 2015; 128:1–39. [PubMed: 26477364]

Volpi SA, Verma-Gaur J, Hassan R, Ju Z, Roa S, Chatterjee S, Werling U, Hou H Jr, Will B, Steidl U, et al. Germline deletion of Igh 3′ regulatory region elements hs 5, 6, 7 (hs5-7) affects B cell-specific regulation, rearrangement, and insulation of the Igh locus. J Immunol. 2012; 188:2556–2566. [PubMed: 22345664]

Xiang Y, Park SK, Garrard WT. A major deletion in the Vk-Jk intervening region results in hyperelevated transcription of proximal Vk genes and a severely restricted repertoire. J Immunol. 2014; 193:3746–3754. [PubMed: 25187654]

Yancopoulos GD, Alt FW. Developmentally controlled and tissue-specific expression of unrearranged VH gene segments. Cell. 1985; 40:271–281. [PubMed: 2578321]

Yancopoulos GD, Desiderio SV, Paskind M, Kearney JF, Baltimore D, Alt FW. Preferential utilization of the most JH-proximal VH gene segments in pre-B-cell lines. Nature. 1984; 311:727–733. [PubMed: 6092962]

Yancopoulos GD, Blackwell TK, Suh H, Hood L, Alt FW. Introduced T cell receptor variable region gene segments recombine in pre-B cells: evidence that B and T cells use a common recombinase. Cell. 1986; 44:251–259. [PubMed: 3484682]

Zhang Y, Liu T, Meyer CA, Eeckhoute J, Johnson DS, Bernstein BE, Nusbaum C, Myers RM, Brown M, Li W, Liu XS. Model-based analysis of ChIP-seq (MACS). Genome Biol. 2008; 9:R137. [PubMed: 18798982]

Zhao L, Frock RL, Du Z, Hu J, Chen L, Krangel MS, Alt FW. Orientation-specific RAG activity in chromosomal loop domains contributes to Tcrd V(D)J recombination during T cell development. J Exp Med. 2016; 213:1921–1936. [PubMed: 27526713]

Author Manuscript Author Manuscript Author Manuscript Author Manuscript

Highlights

- V_H-CBEs greatly augment V_H to DJ_H recombination by enhancing V_H accessibility
- A 3C-HTGTS assay provides high-resolution interaction profiles of *Igh* locus sequences
- V_H-CBEs promote prolonged V_H interaction with the V(D)J recombination center
- RAG chromatin scanning and chromatin loop extrusion share key features

Author Manuscript Author Manuscript Author Manuscript Author Manuscript

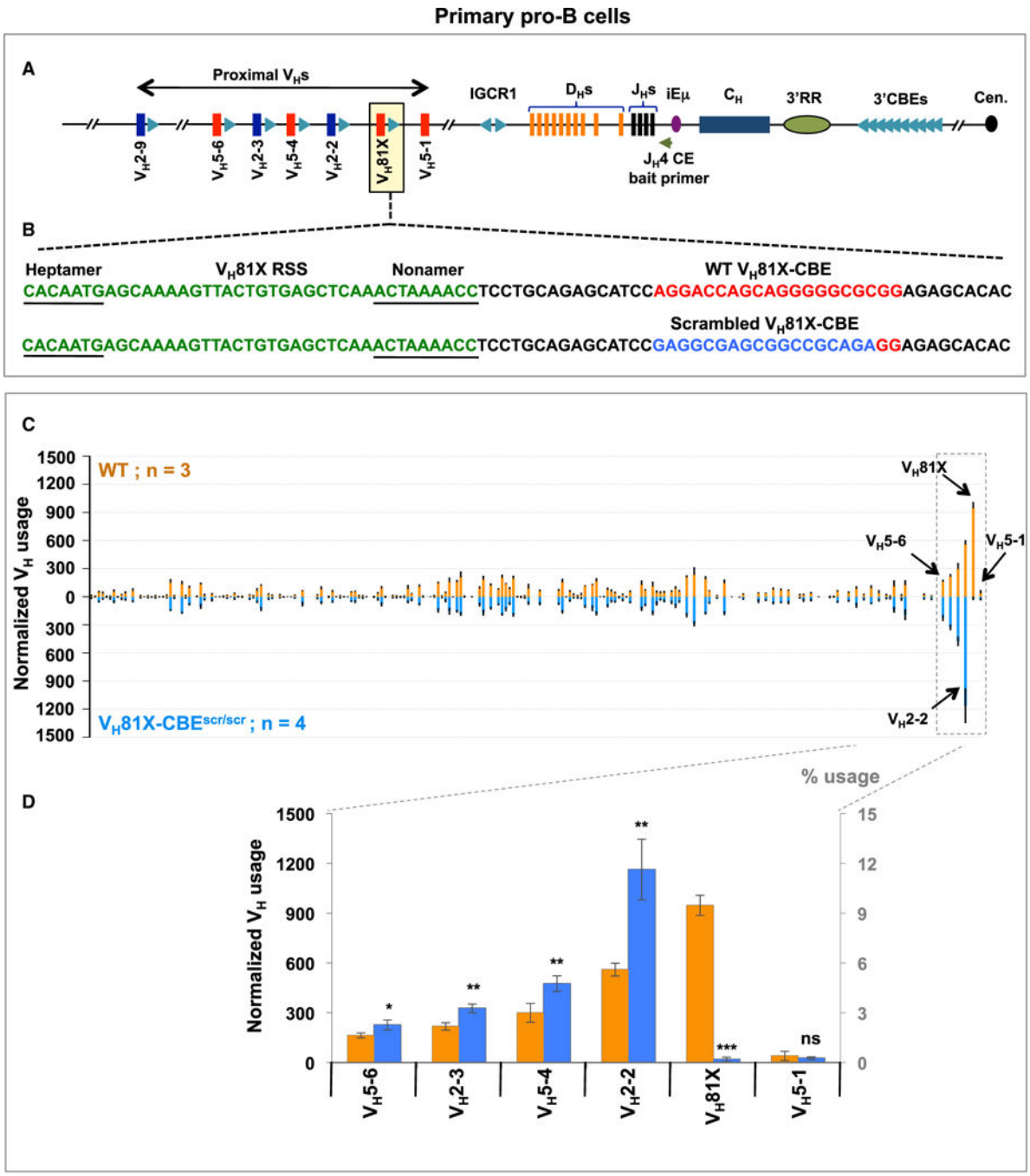

Figure 1. V_H81X-CBE Greatly Enhances V_H81X Utilization in Primary Pro-B Cells

(A) Schematic of the murine *Igh* locus showing proximal V_Hs, Ds, J_Hs, C_H exons, and regulatory elements (not to scale). Red and blue bars represent members of the IGHV5 (V_H7183) and IGHV2 (V_HQ52) families, respectively. Teal blue triangles represent position and orientation of CTCF-binding elements (CBEs). Green arrow denotes position of the J_H4 coding end bait primer used to generate HTGTS-Rep-seq libraries.

(B) Sequence of V_H81X-RSS (green) followed by WT (red) or scrambled (blue) V_H81X-CBE.

Author Manuscript Author Manuscript Author Manuscript Author Manuscript

(C) Relative V_H utilization ± SD in BM pro-B cells from WT (top) or $V_H81X\text{-}CBE^{scr/scr}$ (bottom) mice.

(D) Average utilization frequencies (left axis) and % usage (right axis) of indicated proximal V_H segments ± SD. For analysis, each library was normalized to 10,000 VDJ_H junctions. p values were calculated using unpaired, two-tailed Student's t test, ns indicates $p > 0.05$, *$p \leq 0.05$, **$p \leq 0.01$ and ***$p \leq 0.001$.

See also Figures S1 and S2 and Tables S1, S3, and S4.

Author Manuscript Author Manuscript Author Manuscript Author Manuscript

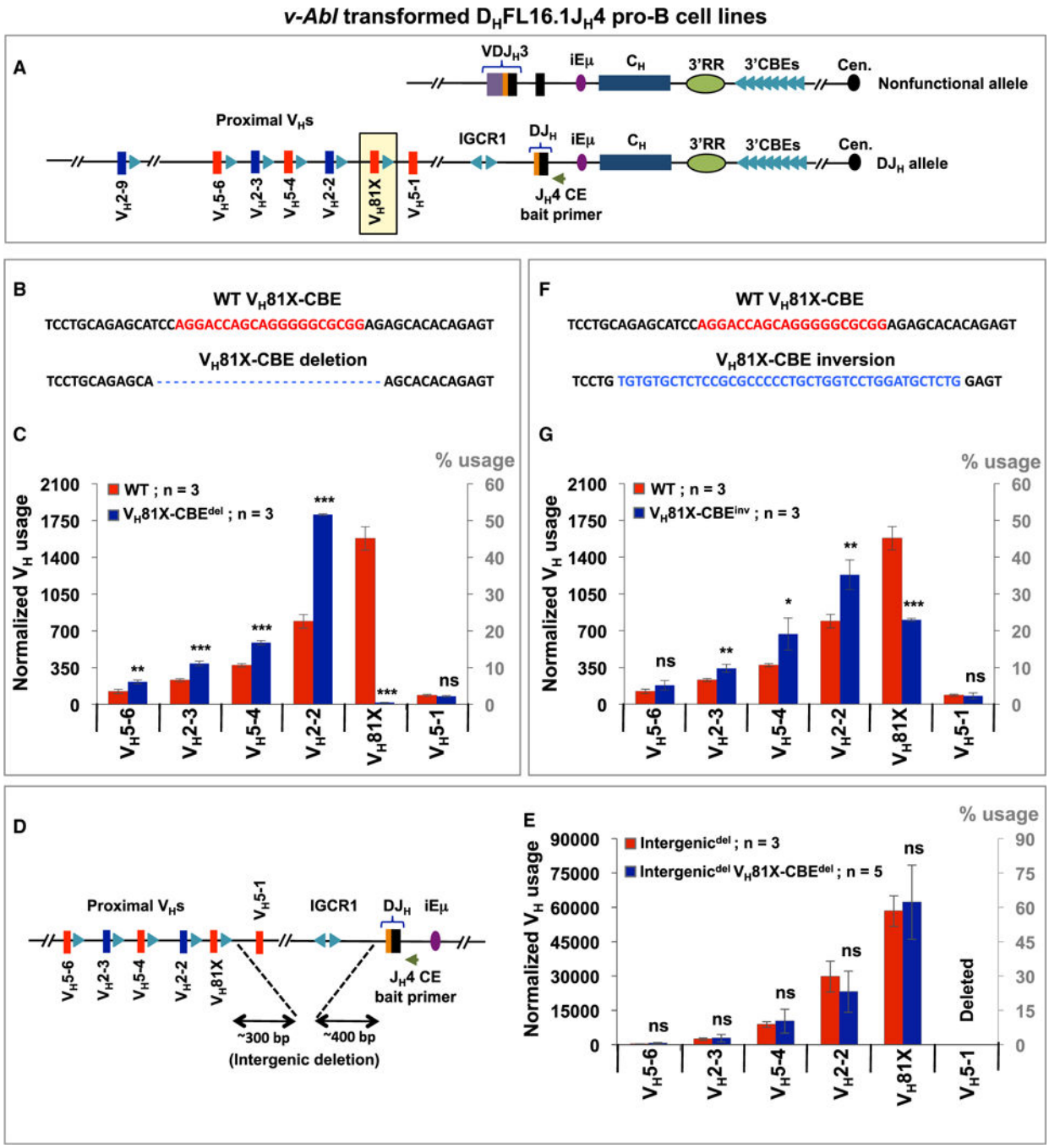

Figure 2. V_H81X-CBE Enhances V_H81X Utilization in DJ_H Rearranged *v-Abl* Pro-B Lines

(A) Schematic representation of the two murine *Igh* alleles in DJ_H rearranged *v-Abl* pro-B cell line (not to scale). One allele (top) harbors a non-productive VDJ_H rearrangement involving a distal V_HJ558 (V_H1-2P) that deletes the proximal V_H domain and is inert for V(D)J recombination. The other allele (bottom) harbors a $D_HFL16.1$ to J_H4 rearrangement (DJ_H allele) that actively undergoes V_H to DJ_H recombination upon RAG induction via G1 arrest. This $D_HFL16.1J_H4$ line served as the parent WT line and was used for all subsequent genetic manipulations.

Author Manuscript Author Manuscript Author Manuscript Author Manuscript

(B) Top line shows the sequence of WT V_H81X-CBE (red) while the bottom line shows V_H81X-CBE deletion (blue dashed line).

(C) Average utilization frequencies (left axis) or % usage (right axis) ± SD of indicated proximal V_Hs in WT and V_H81X-CBE^{del} *v-Abl* pro-B lines; libraries were normalized to 3,500 VDJ_H junctions. As the WT line used for this experiment was the parent of all subsequent V_H-CBE mutant lines, we generated WT repeats at several points over the course of these experiments and used the average data, which were highly reproducible, for this and subsequent panels showing comparisons of mutants with WT controls (see STAR Methods for details).

(D) Schematic of the 101-kb intergenic deletion extending from 302 bp downstream of V_H81X-CBE to 400 bp upstream of the $D_HFL16.1J_H4$ RC in the WT $D_HFL16.1J_H4$ *v-Abl* line and its V_H81X-CBE^{del} derivative.

(E) Average utilization frequencies (left axis) or % usage (right axis) ± SD of indicated proximal V_Hs in Intergenic^{del} and Intergenic^{del} V_H81X-CBE^{del} *v-Abl* lines; libraries were normalized to 100,000 VDJ_H junctions.

(F) Sequence of WT (red) and V_H81X-CBE inversion mutation (blue).

(G) Average utilization frequencies (left axis) or % usage (right axis) ± SD of the indicated proximal V_Hs in $D_HFL16.1J_H4$ WT and V_H81X-CBE^{inv} *v-Abl* lines; libraries were normalized to 3,500 VDJ_H junctions. Statistical analyses were performed as in Figure 1. See also Figure S3 and Tables S1, S2, S3, and S4.

Author Manuscript Author Manuscript Author Manuscript Author Manuscript

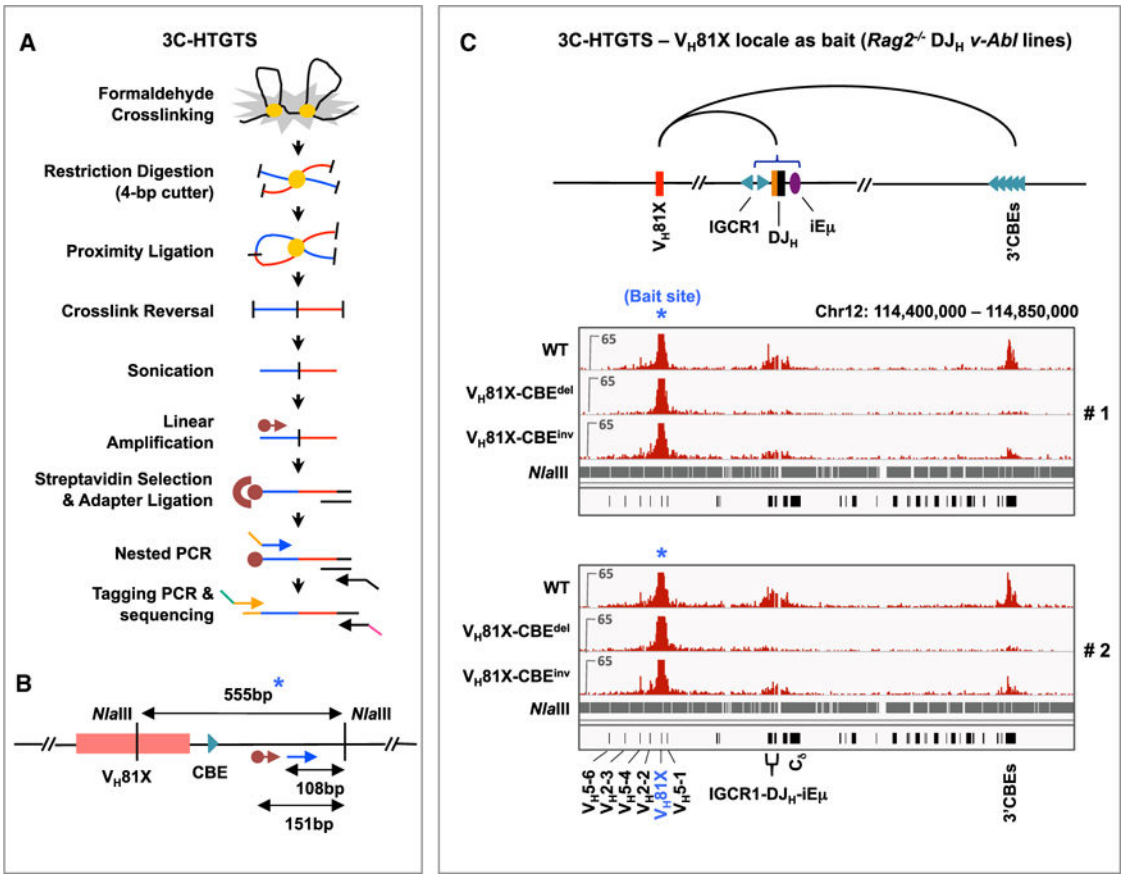

Figure 3. V_H81X-CBE Promotes Interactions of Its Flanking V_H with the DJ_HRC

(A) Schematic representation of the 3C-HTGTS method for studying chromosomal looping interactions of a bait region of interest with the rest of *Igh* locus (see text and STAR Methods for details).

(B) Schematic of the *Nla*III restriction fragment (indicated by a blue asterisk) and the relative positions of the biotinylated (cayenne arrow) and nested (blue arrow) PCR primers used for 3C-HTGTS from V_H81X bait in (C).

(C) Top panel: schematic representation of chromosome interactions of V_H81X-CBE containing *Nla*III fragment with other *Igh* locales. Bottom two panels: 3C-HTGTS profiles of *Rag2*$^{-/-}$ derivatives of control, V_H81X-CBE^{del}, and V_H81X-CBE^{inv} D_HFL16.1J_H4 *v-Abl* lines using V_H81X-CBE locale as bait (blue asterisk). Owing to a D_HFL16.1 to J_H4 rearrangement in the lines, the region spanning IGCR1, DJ_H substrate and iEm appears as a broad interaction peak. As *v-Abl* lines lack locus contraction, we detected few substantial interactions with the upstream *Igh* locus beyond the most proximal V_Hs (see legend of Figure S3). Two independent datasets are shown from libraries normalized to 105,638 total junctions.

See also Table S4.

Author Manuscript Author Manuscript Author Manuscript Author Manuscript

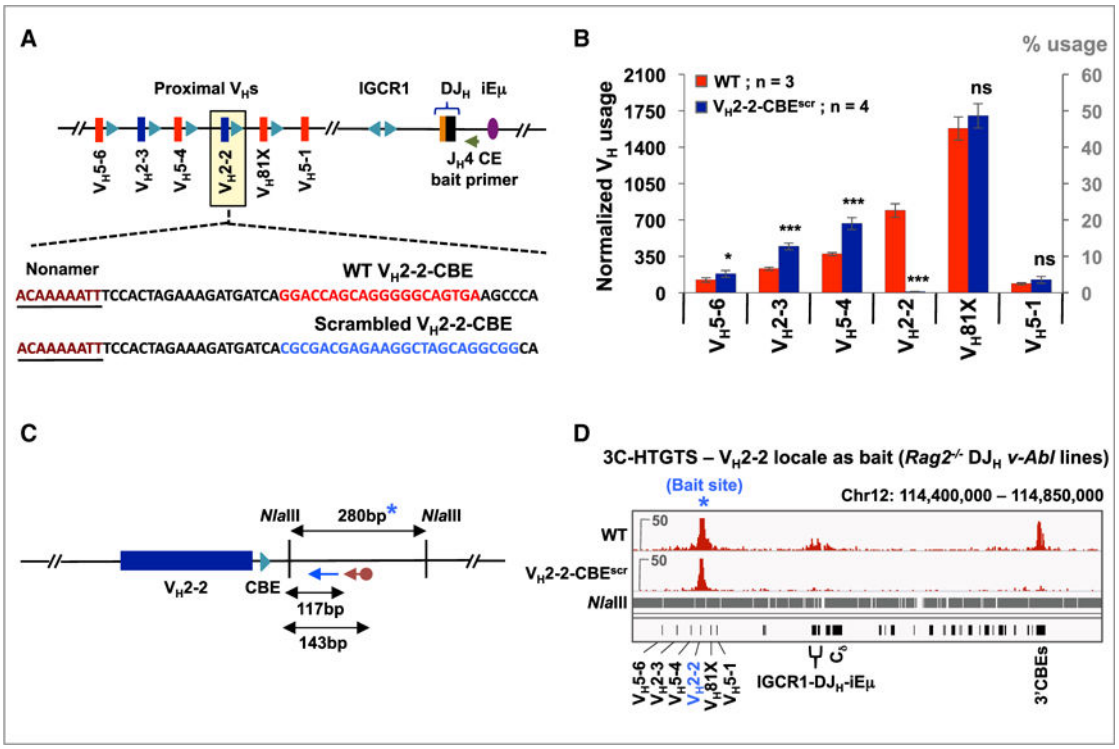

Figure 4. V(D)J Recombination of V_H2-2 Is Critically Dependent on Its Flanking CBE

(A) Sequence of WT V_H2-2-CBE (red) and its scrambled mutation (blue).

(B) Average utilization frequencies (left axis) or % usage (right axis) ± SD of indicated proximal V_Hs in WT and V_H2-2-CBE^{scr} *v-Abl* lines. Each library was normalized to 3,500 VDJ_H junctions. Statistical analyses were performed as in Figure 1. See also Figure S4A and Table S1.

(C) Illustration of *Nla*III restriction fragment (blue asterisk) and relative positions of biotinylated (cayenne arrow) and nested (blue arrow) primers used for 3C-HTGTS analyses in (D). Due to repetitive sequences in the restriction fragment that harbors V_H2-2-CBE, the downstream flanking restriction fragment was used as bait.

(D) Representative 3C-HTGTS interaction profiles of V_H2-2 locale (blue asterisk) in *Rag2*$^{-/-}$ control and V_H2-2-CBE^{scr} *v-Abl* lines, plotted from libraries normalized to 84,578 total junctions. See Figure S4B for an independent repeat.

See also Tables S3 and S4.

Author Manuscript Author Manuscript Author Manuscript Author Manuscript

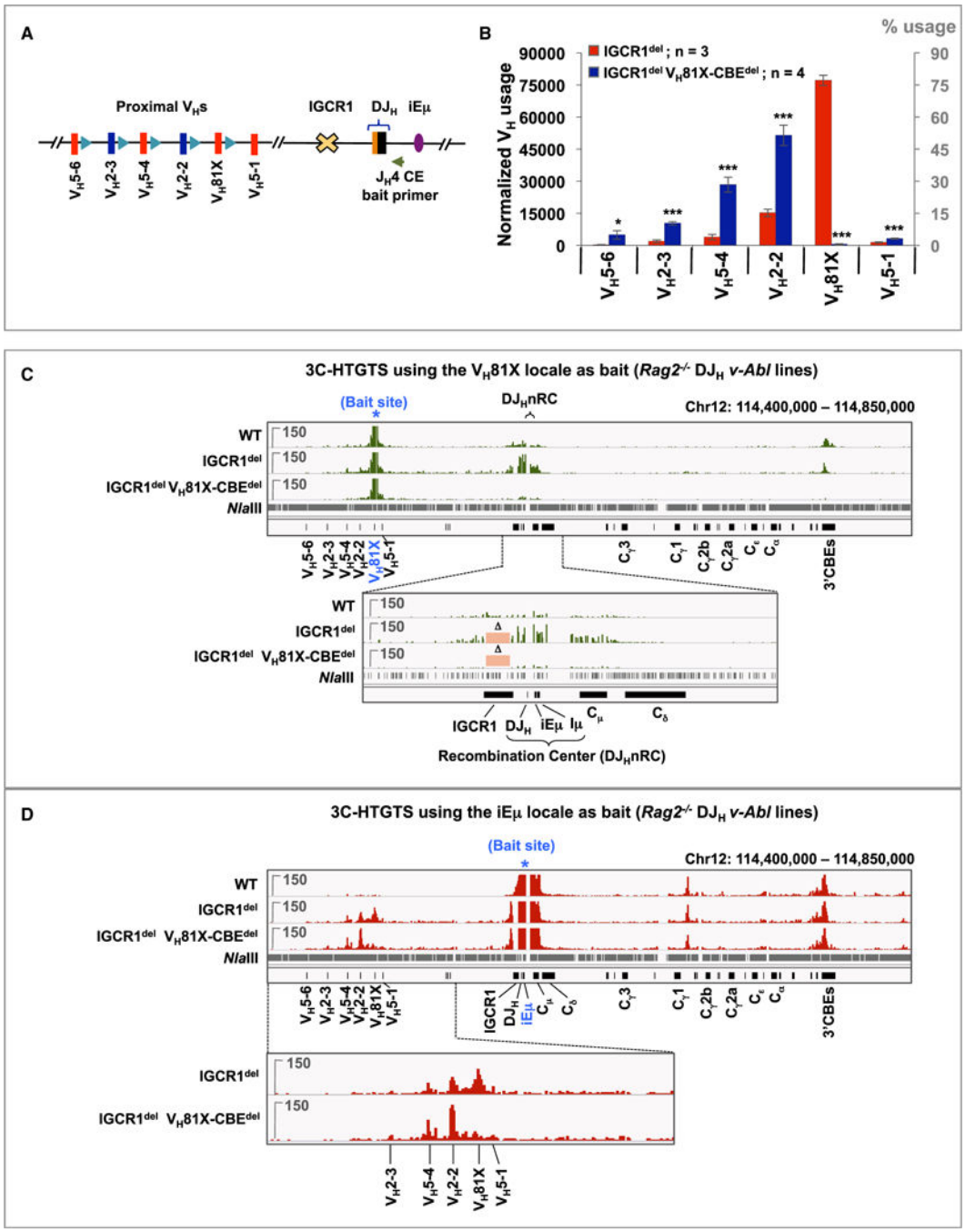

Figure 5. V_H81X-CBE Is Required for Dominant V_H81X Usage in the Absence of IGCR1

(A) Schematic of 4.1 kb IGCR1 deletion.

(B) Average utilization frequencies (left axis) or % usage (right axis) ± SD of proximal V_Hs in IGCR1^{del} and IGCR1^{del} V_H81X-CBE^{del} *v-Abl* lines. Each library was normalized to 100,000 VDJ_H junctions. Statistical analyses were performed as in Figure 1. See also Figures S5A and S5B and Tables S1 and S2.

(C) Representative 3C-HTGTS interaction profiles of V_H81X bait (blue asterisk) in *Rag2*$^{-/-}$ control, IGCR1^{del}, and IGCR1^{del} V_H81X-CBE^{del} $D_HFL16.1J_H4$ *v-Abl* lines performed

Author Manuscript Author Manuscript Author Manuscript Author Manuscript

using the strategy shown in Figure 3B, plotted from libraries normalized to 106,700 total junctions. Bottom panel shows a zoom-in of the region extending from upstream of IGCR1 to downstream of Cd exons. Pink rectangles marked with “D” indicate the IGCR1 region deleted in the IGCR1^{del} and IGCR1^{del} V_H81X-CBE^{del} lines. See Figure S5C for an additional repeat.

(D) Representative 3C-HTGTS interaction profiles of iEm bait (blue asterisk) in *Rag2*$^{-/-}$ *v-Abl* DJ_H lines of the indicated genotypes following *Nla*III digest using the strategy shown in Figure S5D. Each library was normalized to 273,547 total junctions. Bottom: zoom-in of the proximal V_H region. See Figure S5D for an independent repeat and Figure S6 for related repeats.

See also Figure S7 and Tables S3 and S4.

Author Manuscript Author Manuscript Author Manuscript Author Manuscript

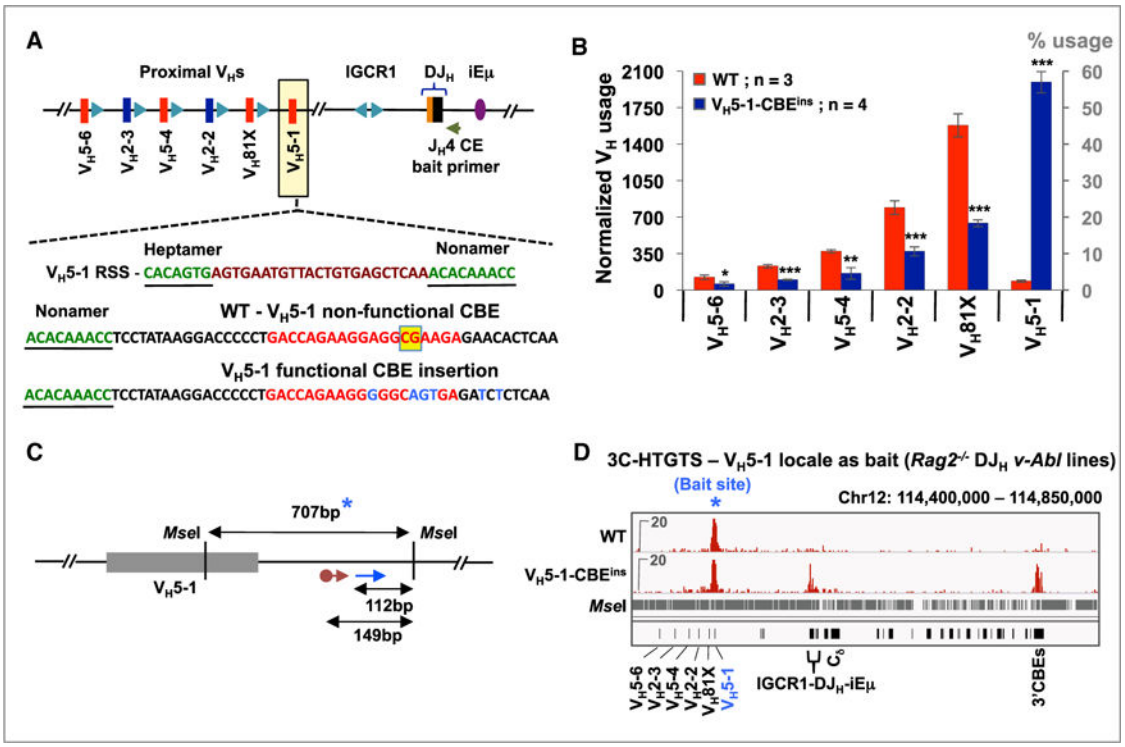

Figure 6. Restoration of a CBE Converts V_H5-1 into the Most Highly Rearranging V_H

(A) Schematic showing the sequence of V_H5-1-RSS and its downstream non-functional, "vestigial" CBE. The yellow shaded box highlights the CpG island that is methylated in normal pro-B cells. Bottom sequence shows the four nucleotides mutated (highlighted in blue) to eliminate the CpG island and restore consensus CBE sequence. Two additional nucleotides were mutated just downstream of the CBE to generate a BglII site for screening.

(B) Average utilization frequencies (left axis) or % usage (right axis) ± SD of the indicated proximal V_Hs in WT and V_H5-1-CBE^{ins} *v-Abl* lines. Each library was normalized to 3,500 VDJ_H junctions. Statistical analyses were performed as in Figure 1. See also Figure S4C and Table S1.

(C) Illustration of the *Mse*I restriction fragment (blue asterisk) and the relative positions of biotinylated (cayenne arrow) and nested (blue arrow) primers used for 3C-HTGTS analyses in (D).

(D) Representative 3C-HTGTS interaction profiles of the V_H5-1 locale (blue asterisk) in *Rag2*$^{-/-}$ control and V_H5-1-CBE^{ins} *v-Abl* lines, plotted from libraries normalized to 37,856 total junctions. See Figure S4D for an independent repeat.

See also Figure S7 and Tables S3 and S4.

Author Manuscript Author Manuscript Author Manuscript Author Manuscript

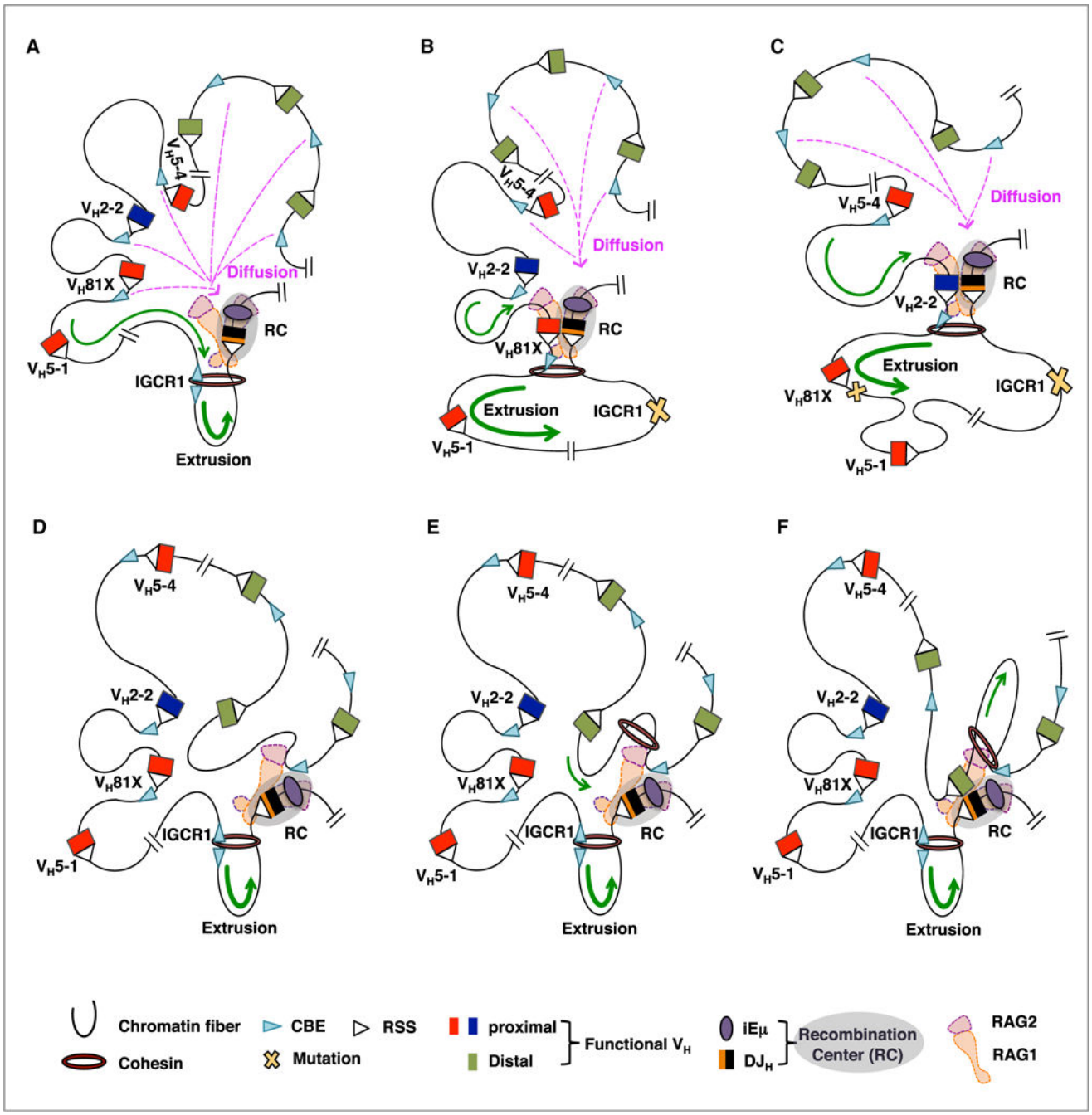

Figure 7. Model for RAG Chromatin Scanning via Loop Extrusion

Figure shows a working model for potential roles of V_H-associated CBEs during RAG scanning over chromatin. Numerous variations of the model are conceivable.

(A) From its location in the initiating RC, RAG linearly scans cohesin-mediated extrusion loops proceeding through Ds, to allow their utilization; but is largely impeded further upstream by the IGCR1 anchor. After formation of a DJ_HRC, residual lower level scanning of upstream sequences beyond the IGCR1 impediment allows the most proximal V_H-CBEs to mediate direct association with the DJ_HRC enhancing utilization of their associated V_H.

Author Manuscript Author Manuscript Author Manuscript Author Manuscript

V_Hs further upstream likely access the DJ_HRC by diffusion with proximal CBEs also enhancing DJ_HRC interactions and flanking V_H utilization.

(B) In the absence of IGCR1, loop extrusion progresses upstream allowing RAG to scan the most proximal V_Hs where associated CBEs promote DJ_HRC interaction, accessibility, and dominant over-utilization in V(D)J joins. Utilization is most robust for proximal V_H81X, which provides the first V_H-CBE encountered during linear scanning. V_H5-1 is bypassed due to lack of a CBE. Scanning can sometimes bypass V_H81X-CBE and continues to the first few upstream V_Hs, with their CBEs similarly promoting utilization.

(C) If both IGCR1 and the V_H81X-CBE are mutated, loop-extrusion continues unabated to the V_H2-2-CBE and to progressively lesser extents to immediately upstream V_H-CBEs.

(D–F) CBEs not directly flanking distal V_Hs theoretically also may augment V_H utilization.

(D) A distal V_H locus CBE associates strongly with chromatin or associated factors (e.g., CTCF/cohesin) at the DJ_HRC.

(E) Cohesin rings load near this DJ_HRC-associated distal V_H locus CBE and initiate loop extrusion.

(F) Loop-extrusion allows RAG to scan downstream (or upstream, not illustrated) V_Hs lacking directly associated CBEs from the DJ_HRC where the active/transcribed chromatin in which they lie facilitates access for V(D)J recombination (see text for more details and relevant references.

See also Figure S1.